SEISMIC BEHAVIOR OF STEEL I-BEAMS MODIFIED BY A WELDED HAUNCH AND REINFORCED WITH GLASS FIBER REINFORCED POLYMERS

A Thesis Submitted to
The Graduate School of Engineering and Sciences of
İzmir Institute of Technology
in Partial Fulfillment of the Requirements for the Degree of

MASTER OF SCIENCE

in Civil Engineering

by
Timur ÖZDEMİR

October 2009

İZMİR

We approve the thesis of **Timur ÖZDEMİR**

Assist. Prof. O. Özgür EĞİLMEZ
Supervisor

Assist. Prof. Cemalettin DÖNMEZ
Committee Member

Assoc. Prof. Metin TANOĞLU
Committee Member

05 October 2009

Prof. Gökmen TAYFUR
Head of the Department of Civil Engineering

Assoc. Prof. Talat YALÇIN
Dean of the Graduate School of Engineering and Sciences

ACKNOWLEDGEMENTS

I would like to express the deepest appreciation to my supervisor, Assist. Prof. Dr. O. Özğür EĞİLMEZ, who has the attitude and encouragement: he continually and convincingly conveyed a spirit of adventure in regard to this research, and an excitement in regard to teaching.

The support of Assist. Prof. Dr. Cemalettin DÖNMEZ and Assoc. Prof. Dr. Metin TANOĞLU were keys in helping manage this study.

I would also like to show my gratitude to my family for their support, endless confidence and love.

ABSTRACT

SEISMIC BEHAVIOR OF STEEL I-BEAMS MODIFIED BY A WELDED HAUNCH AND REINFORCED WITH GLASS FIBER REINFORCED POLYMERS

Flange and web local buckling in beam plastic hinge regions of welded steel moment frames (SMF) can prevent beam-column connections to achieve adequate plastic rotations under earthquake-induced forces. As the use of fiber reinforced polymers (FRP) have increased in strengthening and repair of steel members in recent years, using FRPs in stabilizing local instabilities have also attracted attention. Generally, high modulus carbon FRP (CFRP) laminates, with elastic modulus similar to that of steel, are preferred in strengthening applications. On the other hand, glass FRP (GFRP) has a much smaller modulus than that of steel, typically one order of magnitude less, which limits its use in strengthening applications. However, this modulus mismatch is an asset when the primary goal is to stabilize inelastic local buckling with the least possible strength increase in the section. In a steel-GFRP hybrid system, while the low modulus of GFRP will not allow a significant strength increase in the beam, the flexural strength of GFRP can provide bracing to the underlying steel, which is flowing plastically. In this research study, the cyclic behavior of steel beams modified by a triangular haunch welded to the beam bottom flange only and reinforced with GFRP laminates at beam flanges have been investigated by finite element analysis (FEA). Cantilever I-sections with flange-web slenderness ratios higher then those stipulated in current seismic design specifications are analyzed under reversed cyclic loading. Both bare beam sections and sections reinforced with GFRP are investigated. The effects of GFRP thickness, width, and length on stabilizing local buckling are investigated. The flexural resistance of the beams at column face, interlaminar shear stresses in GFRP strips, and shear stresses at beam-GFRP binding surface are examined. The results reveal that the plastic rotation capacity of steel beams can be enhanced by the use of GFRP strips.

ÖZET

POLİMERLE GÜÇLENDİRİLMİŞ CAM ELYAF İLE DESTEKLENMİŞ, KEMER TAKVİYELİ ÇELİK I KİRİŞLERİNİN SİSMİK DAVRANIŞI

Moment aktaran kaynaklı çelik çerçevelerin kiriş-kolon birleşim bölgelerinde kirişlerde oluşan başlık ve gövde mevzi burkulmaları, birleşimlerin deprem yükleri altında yeterli plastik dönme kapasitelerine ulaşmalarını engelleyebilmektedirler. Polimerle güçlendirilmiş elyafların (PGE) çelik elemanların onarılması ve güçlendirilmesi uygulamalarında kullanımlarına sık sık rastlanılmaktadır. Bunların yanı sıra, PGE malzemeler çelik elemanların mevzi burkulmalarının önlenmesi veya geciktirilmesi amacıyla da son yıllarda kullanılır olmuşlardır. Güçlendirme uygulamalarında genel olarak elastik modülü çeliğinkine yakın olan karbon PGE (PGKE) kullanılmaktadır. Elastik modülü çeliğinkinin yaklaşık onda biri kadar olan cam PGE'ler (PGCE) ise güçlendirme uygulamalarında tercih edilmezler. Ancak elastik modülündeki bu farklılık, amaç kapasiteyi artırmadan mevzi burkulmaların önlenmesi olunca bir avantaja dönüşmektedir. Bir çelik-PGCE karma sisteminde PGCE'nin düşük modülü kapasitenin büyük oranda artmasına olanak vermezken, PGCE'nin eğilme mukavemeti bağlı olduğu çeliği burkulmalara karşı takviye edebilmektedir. Bu çalışmada kiriş başlıkları PGCE ile güçlendirilmiş ve sadece kiriş alt başlığına kaynaklanan üçgen kemerli takviye ile modifiye edilmiş çelik kirişlerin döngüsel davranışları sonlu elemanlar yöntemiyle incelenmiştir. Mevcut deprem yönetmeliklerinde belirtilenlere göre daha narin oranlara sahip konsol çelik I-kesitlerin çözümlemeleri döngüsel yükleme altında yapılmıştır. PGCE ile güçlendirilmiş ve güçlendirilmemiş çıplak kirişlerin davranışları incelenerek karşılaştırılmıştır. Mevzi burkulma stabilizasyonunda, PGCE'lerin uzunluk, genişlik ve kalınlık etkileri araştırılmış; kiriş-PGCE arayüzündeki kesme gerilmesi, PGCE katmanları arasındaki kesme gerilmesi ve kolon yüzündeki kiriş eğilme direnci irdelenmiştir. Bu çalışmada elde edilen sonuçlar PGCE malzemesinin çelik kirişlerin plastik dönme kapasitesini geliştirilebileceğini göstermektedir.

TABLE OF CONTENTS

LIST OF FIGURES

LIST OF TABLES

CHAPTER 1

INTRODUCTION

1.1 Research Overview and Objectives

Seismic design concept for welded steel moment frames (SMF) is generally based on the strong column-weak beam approach. In this way, the majority of the energy dissipation is anticipated to occur by inelastic deformations in the beams through the formation of plastic hinges near beam-column connections. Generally, most important thing is that seismic design of new SMF reaches a higher interstory drift angle in magnitude without important strength reduction or increase of stability; thereby providing a ductile behavior under earthquake induced forces (AISC 2005b, BIB 2006, Eurocode-8 2003, FEMA 2000a).

The ductility of welded beam to column connection is depended on many things. First one is fracture of the beam flange to column groove weld, other thing of effecting ductility is lateral torsional buckling (LTB) and the most important one is to be listed is flange and web local buckling (FLB and WLB). The January 1994 Northridge earthquake damaged a variety of building types throughout greater Los Angeles. Perhaps the most shocking pattern of structural damage involved brittle failures at beam-to-column connections in steel moment frames for flange and web local buckling. After the 1994 Northridge (US) and 1995 Kobe (Japan) earthquakes many engineer and researcher investigated about stress reduction factors and trying to increase welding procedures to cope with the brittle weld fractures in order to augment the plastic rotation capacity of welded connections (Nakashima, et al. 1998, SAC 1996). In any event, beam column connections achieved barely passable plastic rotation capacity does not catch the limits because of elastic local bucklings. This connection is that top and bottom flanges of the beam are welded directly to the column by full penetration groove welds, beam web is bolded to a shear plate, which is attached to the column by welding. In addition to these design codes and modification methods show the researchers how to

develop existing and new SMF systems by some techniques one of this is welded haunch (WH). Existing steel moment frames is under this threat that need to be improved. (AISC 2001, FEMA 2000a, FEMA 2000b).

Throughout the large plastic rotations, Okazaki et al. (2006) and Nakashima et al. (2002 and 2003) have investigated that instabilities can be controlled for beam in SMF in favor of width thickness ratio and unbraced length to control instabilities. It is the most important, expensive and difficult thing is to be retrofitting of local buckles. The significant aim is to improvement of local inelastic stabilities I-beams in SMF. In that way, awkward repair works and cost can be gotten rid of.

As the use of fiber reinforced polymers (FRP) have increased in strengthening and repair of steel members in recent years, using FRPs in stabilizing local instabilities have also attracted attention (Accord and Earls 2006). The high stiffness-to-weight and strength-to-weight ratios of FRP materials, combined with their resistance to corrosion have increased their use in repair and strengthening of steel structures. Generally, high modulus carbon FRP (CFRP) laminates, with elastic modulus similar to that of steel, are preferred in repair and strengthening application of steel sections. On the other hand, in a steel-glass FRP (GFRP) composite system the low modulus of GFRP as compared to that of steel can be an asset in stabilizing flange and web local buckling during plastic hinge formations. While the low modulus of GFRP will not allow a significant strength increase in the steel section, its compressive strength will enable GFRP strips to maintain their flexural strength to provide bracing to the underlying steel, which is flowing plastically. This type of a composite action will enhance the plastic rotation capacity of the plastic hinge region; provided that an early debonding or GFRP fracture do not control the behavior.

In this study it is aimed to enhance the cyclic behavior of existing welded steel moment frame connections rehabilitated by a triangular haunch welded to the beam bottom flange through the use of GFRP materials. GFRPs were applied in the region of beam plastic hinges. Figure 1.1 shows GFRP strips placed on top and bottom of beam flanges, both at inside and outside of the welded haunch region for the top flange and only at outside of welded haunch region for the bottom flange.

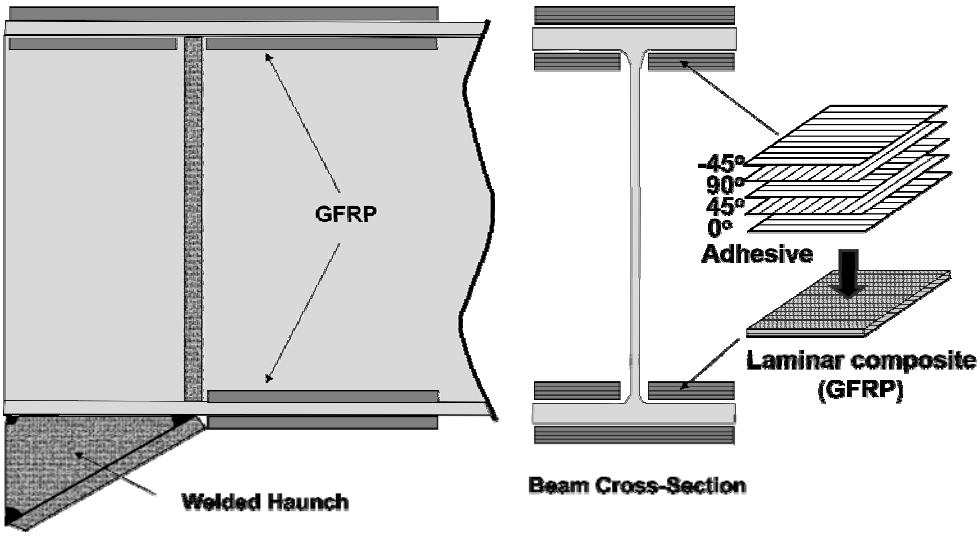

Figure 1.1 The Hybrid System of Beam-GFRP Material

The research consisted of laboratory investigations and finite element analysis (FEA) studies. Experiments consisted of cyclically loaded cantilever I-beams rehabilitated with a triangular haunch at the beam bottom flange with and without GFRP. Small-scale standard tests on polymers and GFRP were also conducted to determine the mechanical properties of GFRP and the interface surface between GFRP and steel. FEA studies consisted of studying the reversed cyclic behavior of several cantilever I-sections with a triangular haunch at the bottom flange and flange-web slenderness ratios (FSR and WSR) higher then those stipulated in current design specifications. Both bare beam sections and sections reinforced with GFRP are investigated. The behavior of bare steel sections were then compared with those of steel sections reinforced with GFRP strips. The effect of GFRP thickness, width, and length on stabilizing local buckling is investigated. The flexural resistance of beams at column face, together with interlaminar shear stresses in GFRP strips and shear stresses at the beam-GFRP binding surface are examined. Recommendations on the use of GFRP materials in beam plastic hinge region to mitigate local buckling and improve the cyclic behavior of I-beams are provided.

1.2 Study Overview

This analytical study is presented in 5 chapters. Following this introduction, Chapter 2 presents a brief background on rehabilitation techniques of exiting steel moment frame connections, fiber reinforced polymers, and steel-GFRP systems. Chapter 3 provides an overview of the FEA studies, whereas Chapter 4 presents the FEA results. Finally, a summary of the research investigation and recommendations are provided in Chapter 5.

CHAPTER 2

BACKGROUND

2.1. Introduction

The 1994 Northridge and 1995 Kobe earthquakes have led to a major change in the seismic design of SMF connections. National Institute of Standards and Technology (NIST), the American Institute of Steel Construction (AISC), the Federal Emergency Management Agency (FEMA), the University of California at San Diego, the University of Texas at Austin, and Lehigh University have undergone a project that aims at enhancing the seismic performance of the connections that were build before the Northridge earthquake. This project is made up of experimental, analytical and numerical studies (SAC 1996, AISC 2001, Uang, et al. 2000, Yu, et al. 2000). Consequently, in order to enhance the strength, stiffness, ductility and deformation capacity of the connections, new design guidelines regarding construction have been formed and new modification methods for current SMFs have been developed (FEMA 2000b).

To be able to keep the plastic hinging of the beam away from the face of the column, new design guidelines include three main design strategies including strengthening or weakening the beams: Reduced Beam Section (RBS), Welded Haunch (WH) and Bolted Bracket (BB) modifications (AISC 2001). The consequence of keeping the occurrence of the plastic hinge away from the column is the limitation of the maximum moment at the column face and, thus, reduction of the risk of brittle weld fractures near the edge of the beam flange to column groove weld. In this study, only the WH modifications shall be considered. Gross et al. (AISC 2001) reports that in WH modifications, strengthening was generally carried out by using the haunch on the bottom side of the beam and weakening methodology was the reduction of the beam section near the column face in conjunction with increasing the weld quality.

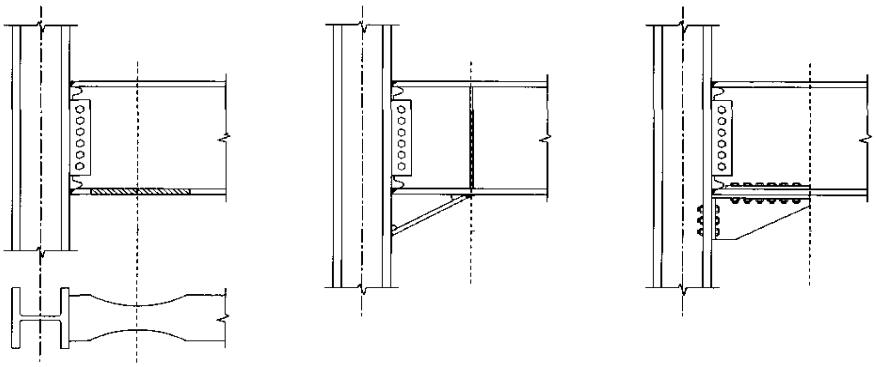

Figure 2.1 Types of Modifications
(Source: AISC Steel Design Guide 2003)

The stress reduction and better weld quality at the beam-column connections of existing SMFs can now be satisfactorily accomplished to overcome the brittle weld fractures observed during the 1994 Northridge and 1995 Kobe earthquakes. However, mitigation of inelastic instabilities is still an issue and local member buckling can still prevent the connection to achieve adequate plastic rotations. Now that the use of advanced composite materials in steel structures has been increasing rapidly, using FRP composite materials in mitigation of local buckling so as to increase the plastic rotation capacities is in consideration (Accord and Earls 2006).

This chapter includes background information on three main topics. The first part will be about the SMF modified WH connection. The second part is made up of general information on steel-FRP composite hybrid systems and the mechanical properties of FRP composite materials utilized in enhancing the seismic performance of beam-column connections. Lastly, information on erstwhile works that are in relation to steel-FRP composite hybrid systems is given.

2.2. Post-Northridge SMF Connection Background

2.2.1. Welded Haunch (WH) Modification Method

In Figure 2.2, we can see the details of the welded haunch (WH) connection technique. As the figure illustrates, a triangular haunch is welded to the beam bottom flange so that the beam near the welded connection can be strengthened. According to the reports of SAC (1996), when the welded haunch is used in both top and bottom flanges of the beam, the seismic performance of the beam increased in consideration to one-sided welded haunch connection. However, the existing structures and new constructions based on concrete slab render the usage of WH connection and make the top flange welding difficult since removing the concrete slab around the column requires additional cost and workmanship.

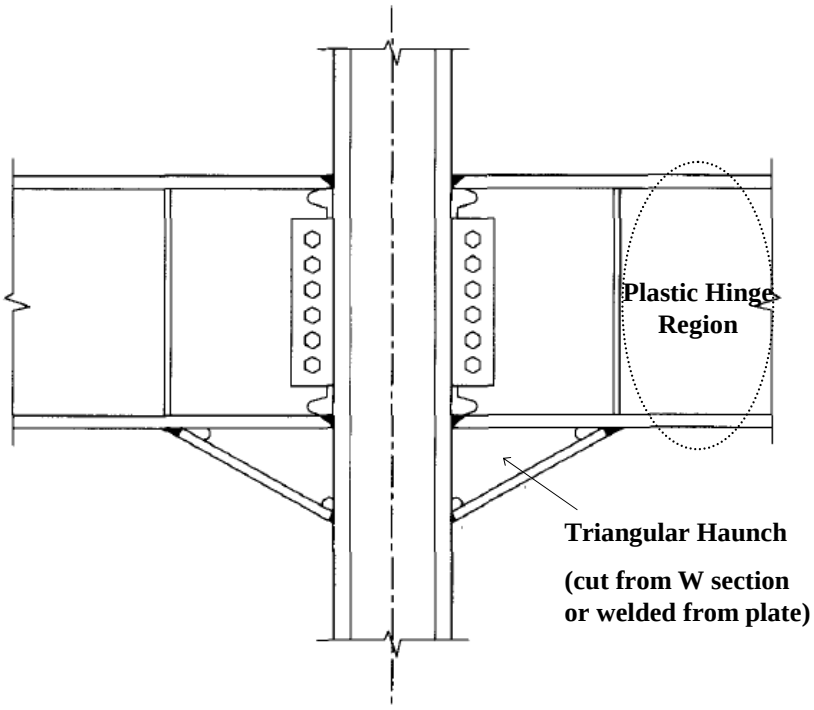

Figure 2.2 Details of Welded Haunch Connection
(Source: AISC Steel Design Guide 2003)

SAC 1996 test results show that adding a welded bottom haunch improves the cyclic performance of the connections as well. In addition, Uang et al. (2000) and Yu et al. (2000) pointed out that utilization of bottom haunch connection renders any modification in existing groove welds unnecessary. In the light of these findings, this study will include adding a triangular haunch only at the bottom side of the beam.

Structurally, the tapered haunch is a flange and web plate or is cut from a structural tee or wide flange section (AISC 2001). Theoretical and experimental study was carried on by Yu and Uang at University of California San Diego (UCSD) (Uang, et al. 2000, Yu, et al. 2000). They discovered that a welded haunch results a change in the beam shear force transfer mechanism. The welded haunch acts as a "diagonal strut". Hereby, the majority of the shear force flows through the haunch flange towards the column. Besides, according to the report by Gross et al. in AISC Design Guide No. 12 (AISC 2001), a pair of beam web stiffeners must be placed at the end of the haunch so that the vertical load that sits on the welded haunch can be distributed to the beam web.

Provided that welded haunch is placed with adequate stiffness and strength, plastic hinge of the beam occurs at the end of the welded haunch hence, tensile stress in the beam-to-column connection weld is reduced.

2.3. Steel-FRP Composite Hybrid System Background

2.3.1. Introduction

For whatever purpose it is intended to be used, the individual properties of the constituent materials must be internalized so that the working principle of steel-fiber composite hybrid systems can be evaluated. In this section, basic information on mechanical properties of fiber, matrix material, binding material used for binding composite material to steel and steel-GFRP hybrid systems shall be given.

2.3.2. Properties of Fiber Material

Polymer composite materials strengthened with fiber are composed of two components: a) fiber, b) binding matrix. Carbon, glass and aramid fibers are usually utilized in industrial applications. Carbon has the highest stiffness and strength values among the all the fibers mentioned above (Cadej, et al. 2004). The range of the elastic modulus of carbon fiber is 230 GPa to 640 GPa (Setunge, et al. 2002). High modulus values are the chief reason for using carbon fiber composites to strengthen and repair applications.

Aramid also has high strength and modulus but a mid-degree stiffness. On the other side, glass fibers are the least stiff and strong yet, they have the price of advantage (Cadei, et al. 2004). The elastic modulus value of glass fibers varies from 70 GPa to 85 GPa (Setunge, et al. 2002).

2.3.3. Properties of Matrix Material

Polymeric matrix is the chief component in composite materials which keeps the fibers together and sustains the composite integrity. The load transfer between the fibers is provided by the matrix. Apart from these properties, matrix acts as a protector against environmental effects (Gibson 1994, Schwartz 2002). Heat fire and chemical resistance of the composite materials are due to the properties of the polymeric matrix (Cadei, et al. 2004).

Epoxies and polyester resins are the most predominantly used polymer matrix (Gibson 1994). The elastic modulus range of matrix varies between 2.5 GPa and 4 GPa, tensile strength is 50 to 85 MPa, and shear strength changes from 13.5 to 20 MPa (Lili, et al. 2008, Egilmez 2007, Cadej, et al. 2004, Boone 2002).

2.3.4. Properties of Fiber Composite Material

The properties of the fiber and matrix, fiber-matrix volume fraction, direction of the fibers and manufacturing methods designate the mechanical properties of fiber composites. Fiber-reinforced composites are most commonly stacked in a number of

layers within laminates. 0°/90°, 0°/+45°/-45°/90° fiber orientations are generally used in fiber applications depending on the purpose of use (Hull and Clyne 2000, Schwartz 2002). A number of simple cross-ply laminates are illustrated in Figure 2.3.

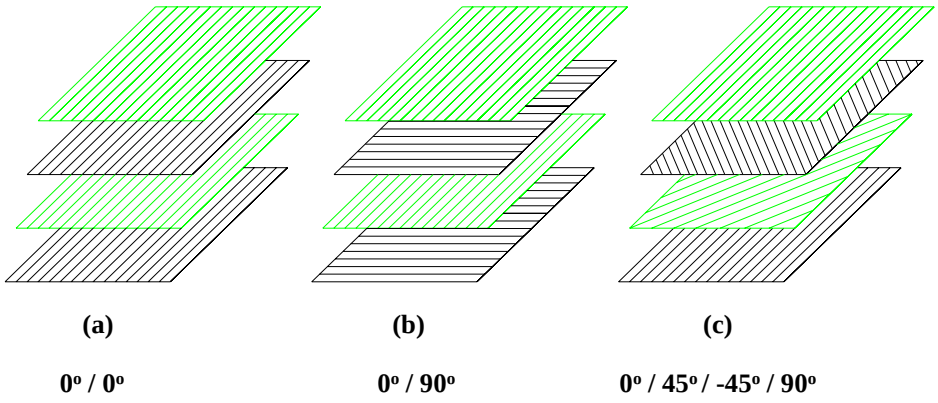

Figure 2.3 Schematic View of Fiber Orientations

2.4. Literature Review of Steel-GFRP Composite Hybrid System

In the recent decades, fiber reinforced polymer (FRP) composite materials have been used to strengthen the steel components (Schnerch et al. 2006, Photiou et al. 2005, Tavakkolizadeh and Saadatmanesh 2003). High modulus carbon and aramid fiber materials which have similarly elastic modulus with that of steel are mainly preferred for this sort of applications. Recently, alongside the applications oriented at strengthening, researches have been oriented at raising the plastic rotation capacity of steel elements via GFRP elements. Yet, not many studies on this subject are avaliable in the literature.

A finite element study by Accord et al. (2006) is the most significant work on stability of local buckling of steel members utilizing GFRP. Accord used a 3-D finite element analyses on cantilever steel I-beams with GFRP strips bearing static loading to

investigate the part GFRP strips play in the plastic rotation capacity and flexural strength in the section of the study. Steel beams with GFRP strips offer a higher plastic rotation capacity that those of bare steel beams and an increase in flexural strength by %25 is confirmed. GFRP strip modelings were conventional shell elements in which the interface materials and GFRP strips were perfectly bounded together and modeled as isotropic elastic materials.

Ekiz et al. (2004)'s experimental study investigated the energy dissipating capacity of double channel members wrapped by carbon fiber reinforced polymers (CFRP) around the plastic hinge regions, under reversed cyclic loading. Two separate wrapping were applied to the members. The first application is that CFRP strips were bonded to the bottom side of the member in the plastic hinge region. The second implementation is that the beam was fully wrapped around the plastic hinge region. According to the test results, CFRP wrapping can increase the size of the yielded plastic hinge region and inhibit occurrence of local buckling.

There is also a finite element study by Sayed-Ahmed (2006). In this study, CFRP strips were located on the compression region of the I-beams and contribution of CFRP strips on delaying the local web buckling is investigated. Steel I-section beams with different web slenderness ratios were analyzed by linear buckling and nonlinear finite element analyses. The results of the parametric study displayed that the use of CFRP strips can lead to the delay of local buckling of the web and this can result in load and strength increase. The ratio of the critical load increase changed from 20% to 48% for different web slenderness ratios.

A experimental study by Photio et al. (2006) involved steel beams that were reinforced with hybrid composites. This study tested the flexural strength capacity of four steel rectangular cross-section beams under four-point loading. Two beams were modified with U-shaped units while the others were strengthened with flat plate units to its tension flange. The flexural capacities of the steel beams were increased using units consisting of hybrid lay-up of CFRP and GFRP composites. Photio et al. (2006) reported that the hybrid lay-up of CFRP and GFRP composite usage visibly improved the capacity of a steel girder to embrace the flexural load.

Apart from Photiou et al. (2006), Schnerch et al. (2007) carried on an analytical study which demonstrated the flexural behavior of steel-concrete composite bridge girders with high modulus CFRP bonded to the tension flange of composite beams

using a structural epoxy adhesive. This study resulted in the presentation of a flexural design procedure. According to the findings, flexural-strengthening beams increased the capacity of stiffness and strength.

In an akin design, the steel-concrete composite sections were reinforced with epoxy-bonded CFRP sheets placed under static loading (Tavakkolizadeh and Saadatmanesh 2003). In this experimental and analytical proceeding, three large-scale composite girders with one, three and five-layered CFRP laminates that were bonded to the tension flange of beams were tested. The results of the experimental survey displayed that the ratio of the girders' ultimate load-carrying capacity showed an increase between 44% and 76% depending on the different number of CFRP layers.

Besides the above-mentioned works, various other studies have been performed on strengthening of steel and steel-concrete composite sections by the use of CFRP (Lenwari, et al. 2005, Rizkalla and Dawood 2006, etc.). These studies showed that the flexural strength of steel sections can be significantly improved via the use of externally bonded CFRP composite materials.

Apart from these, there have also been studies on the properties and fracture modes of adhesives used in steel-composite system (Buyukozturk, et al. 2003, Damatty, et al. 2003, Fawzai, et al. 2006, Taib, et al. 2005a and 2005b, Dawood and Rizkalla 2006). The results of the fracture stresses of adhesive materials showed that it is possible to model adhesive materials via elastic elements.

In addition, a 3-D finite element based study by Alkan (2008) conducted a study on the stability of local buckling of steel members utilizing GFRP composites. Alkan studied on the cantilever steel I-beams that have different slenderness web and flange ratios with GFRP strips. Beams were subjected to cyclic loading to investigate the contribution of GFRP strips to plastic rotation capacity and flexural strength in the section. It is confirmed that steel beams with GFRP strips had higher plastic rotation capacities than bare steel beams'. In this research, the GFRP strips were modeled as layered shell elements. They were modeled as orthotropic elastic materials and perfectly bonded to steel surface.

CHAPTER 3

FINITE ELEMENT MODEL

3.1 Introduction

The three dimensional finite element program ANSYS (2007) was used to conduct FEA studies on the cyclic behavior of beams modified by a triangular haunch welded to the beam bottom flange and reinforced with GFRP strips. Non-linear analysis with respect to both material and geometry was considered. The accuracy of the FEA model was verified by comparing the analysis results with cantilever beam test results conducted at the laboratory and from literature. This verification is presented in the following sections. The basic features of the FEA model, its verification, and sections used in the analyses will be described in this section.

3.2 FEA Model

A half span steel frame model was adopted in the study as shown in Figure 3.1. The column was modeled as a rigid bar; whereas the beam, triangular haunch, and the stiffener at the end of the haunch were modeled using eight-node quadrilateral shell elements with six degrees of freedom per node. This element possesses plasticity, large deflection, and large strain capabilities. The flange and web nodes of the beam and triangular haunch at the column face were coupled to the coinciding column nodes of the rigid column elements in all directions (3 displacements: UX, UY, UX, and 3 rotations: ROTX, ROTY, ROTZ) to form a fixed end connection. The nodes at the bottom flange face of the web and flange of the triangular haunch were coupled to the coinciding bottom flange nodes in all directions to simulate the weld between the beam bottom flange and triangular haunch. The other end of the beam was supported by a roller; unconstrained in the longitudinal direction and constrained in the vertical direction. The beam was laterally restrained (both twist and out-of-plane motion) at mid-span and at the

end with the roller support in order to ensure that lateral-torsional buckling did not control the failure mode. The column was simply supported at the bottom and supported by a roller at the top; unconstrained in the vertical direction and constrained in the longitudinal direction. Both top and bottom of the column were constrained against out of plane motion.

The length of the column and the beam were taken as 4000 mm and 3500 mm, respectively. The mesh sizes for the beam flanges and web were 16.5×20 mm and 47×20 mm in the initial 1/3 of the beam from the fixed end and 16.5×58 and 47×58 mm thereof, respectively. Both geometric and material non-linearity was considered. The yield strength (F_y) and elastic modulus (E) of steel was taken as 345 MPa and 200 GPa, respectively. A yield strength of 345 MPa covers most of the wide flange beams produced after around 1960s (AISC 2002). A bilinear kinematic hardening rule was adopted for the stress-strain behavior of steel, with a secondary stiffness equal to 1/100 of the elastic modulus.

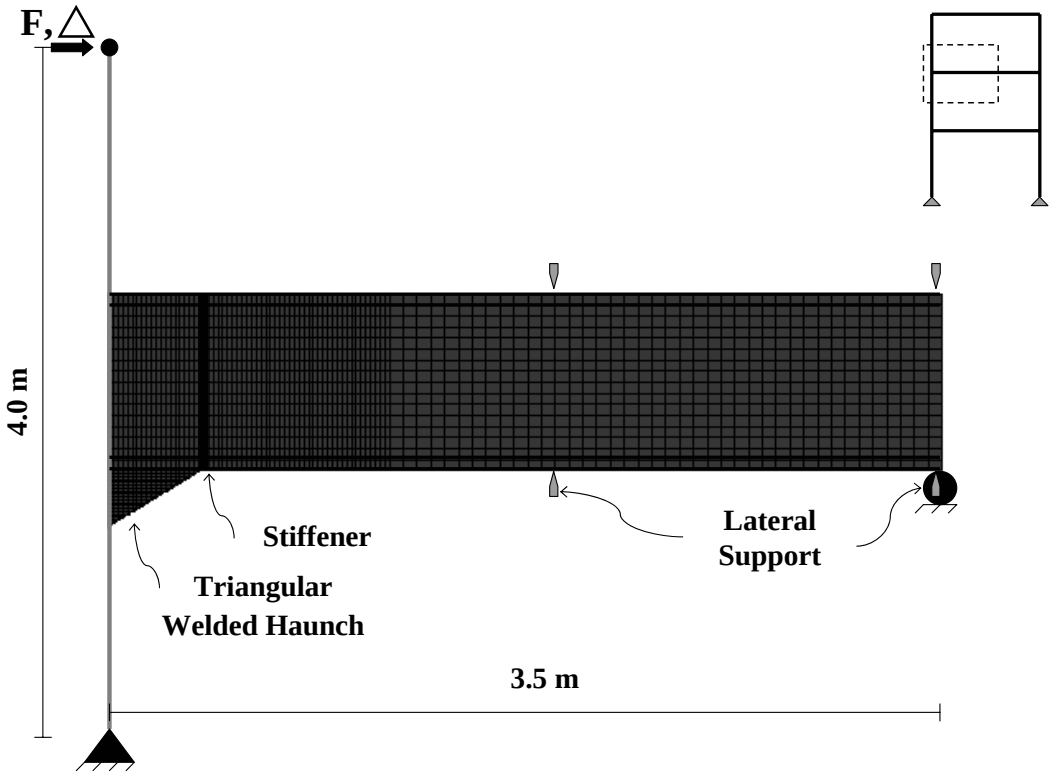

Figure 3.1 Half Span Frame Model

The GFRP laminates and the epoxy resin used to attach the GFRP to the steel surface were jointly modeled using layered eight-node solid elements with three degrees of freedom per node (translations in the nodal X, Y, and Z directions). The initial layer of the element adjacent to the flange shell elements was treated as the epoxy resin and the other layers were treated as GFRP laminates. The thickness of each GFRP layer and epoxy resin were taken as 0.9 mm and 0.5 mm, respectively. The mechanical properties of each layer (epoxy and GFRP) were based on laboratory test results (Güven 2009). The elastic and shear modulus of GFRP laminates were taken as 10000 MPa and 2100 MPa, respectively. The elastic modulus of the epoxy layer was taken as from the manufacturer's brochures as 2600 MPa. Poisson's ratio was assumed as 0.3 for all materials. The finite element model of the cantilever beam with the triangular haunch and GFRP laminates is shown in Figure 3.2.

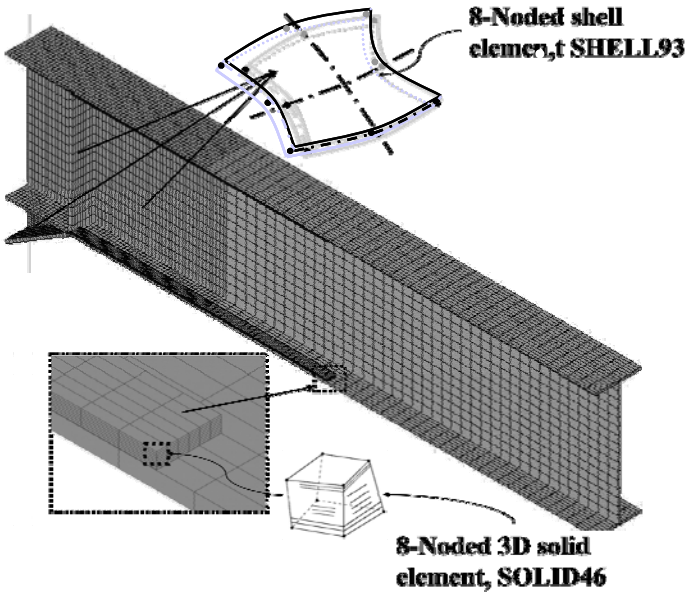

Figure 3.2 FEA Model of Cantilever Beam with Triangular Haunch and GFRP Laminates

3.3 Imperfections

The effects of initial imperfections were also considered in the model, similar to the procedure followed by Accord and Earls (2006). A linear eigenvalue buckling analyses was performed for each beam section prior to non-linear analyses in which the cantilever beam was displaced towards the top flange. The displacement field obtained from the first eigenmode was then scaled by a factor of L/1000 and applied to the model geometry to create the initial imperfections. The factor of L/1000 is selected based on the permissible out of straightness specified in AISC (2005c).

3.4 Loading Sequence

Cyclic loading was applied to the beams as drifts to the tip of the rigid column element, according to the loading sequence shown in Figure 3.3. The rotation, θ, shown in Figure 3.3 represents the rotation of the beam at the fixed end; which is also equal to the rotation of the rigid column element. The sequence is identical to the loading sequence defined in AISC (2005a) for cyclic tests of beam-to-column moment connections in SMF and IMF; except that the initial elastic cycles are omitted.

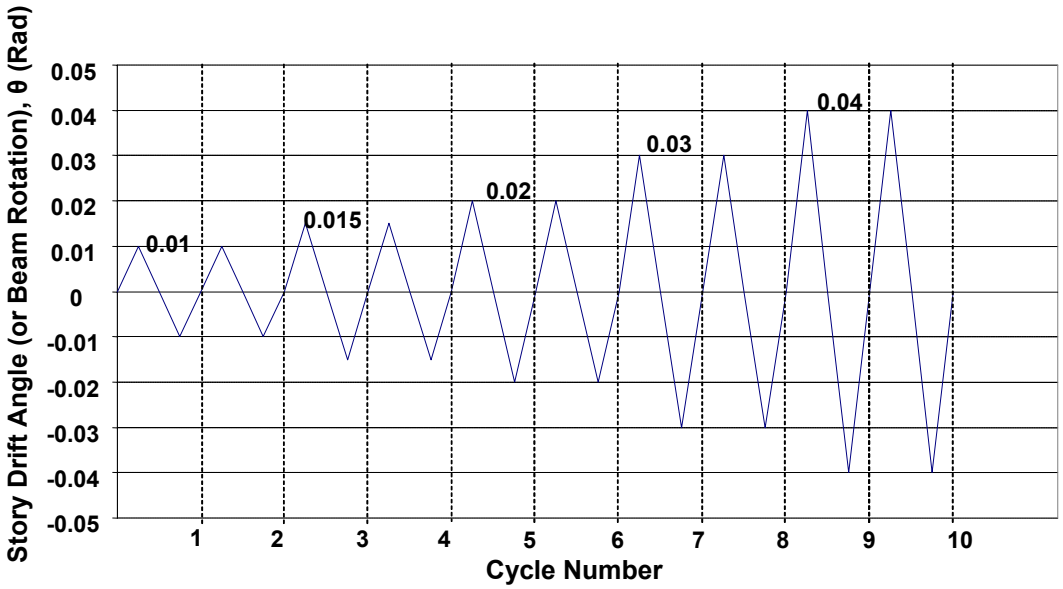

Figure 3.3 Loading Sequence Followed in FEA

3.5 Verification of the FEA Model

The validity of the FEA simulation was verified by comparing the cyclic behavior of a wide flange I-section with that of the FEA simulation. The test used in the verification study was a full-scale cantilever beam test conducted at the structural engineering laboratory of Izmir Institute of Technology. The beam was a European wide flange beam, HE400AA, with a depth of 378 mm, web thickness of 9.5 mm, flange thickness of 13 mm, and width of 300 mm. The fixed end of the beam was modified by a welded haunch at the bottom flange. The cantilever beam was loaded cyclically similar to the loading protocol defined in AISC (2005a) for cyclic tests of beam-to-column moment connections in SMF and IMF. A photograph of the HE400AA beam in the test setup and the loading sequence followed in the test are shown in Figure 3.4 and 3.5, respectively. Due to the fact that the laboratory facilities did not have a strong wall, a strong steel frame was constructed and the test beam was bolted to it as seen in Figure 3.4.

Figure 3.6 shows the load-fixed end rotation behavior of the HE400AA test beam and FEA simulation. The test was stopped at the second cycle of 0.03 radians of rotation when the load started to drop. As can be seen from the figure the FEA model predicted the behavior of the test beam very well. The only slight deviation occurred at the second cycle of 0.03 rad of rotation, where the FEA model reached only up to about 94% of the moment capacity of the test beam at positive rotation. This was probably due to the fact that the connection between the welded haunch stiffener and the flanges was not exactly simulated in the model. In the test beam the 25 mm thick stiffeners were fillet welded to the flanges on both sides. This type of a connection provided a 45-50 mm wide and 130 mm long rigid area on the flanges where the stiffeners were welded. In the FEA model however, the coinciding nodes of the top and bottom elements of the stiffeners were coupled to the flange elements' coinciding nodes along a single line. Although all six degrees of freedoms were coupled, the connection that was simulated in the model was more flexible than the connection provided in the actual beam. Hence, the flanges of the FEA model were more vulnerable to local buckling than the flanges of the actual beam.

Figure 3.4 Photograph of HE400AA Test Specimen in the Test Setup

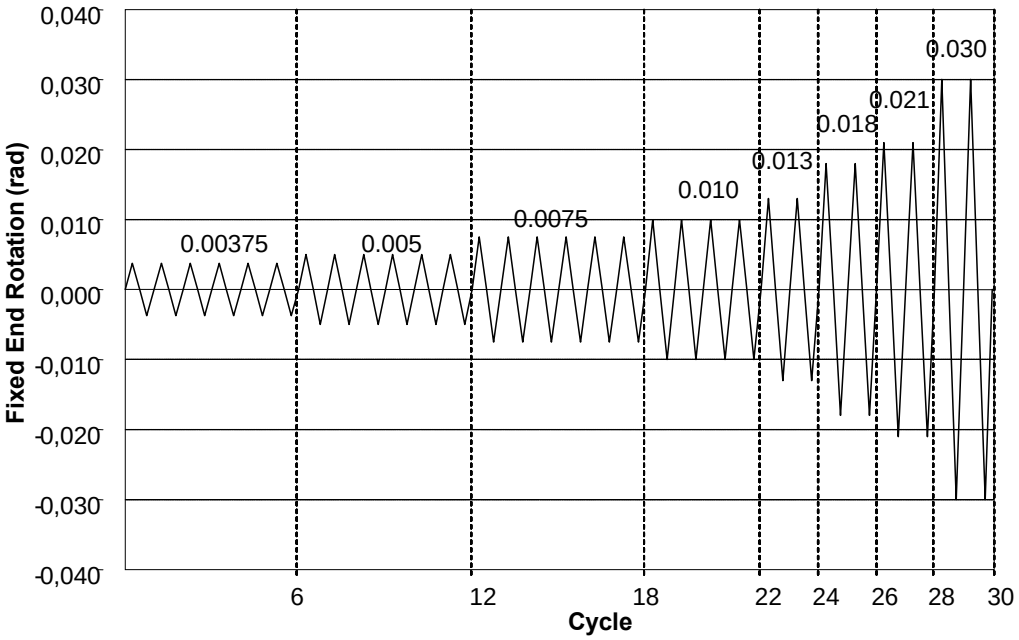

Figure 3.5 Loading Sequence Followed in the Cyclic Test

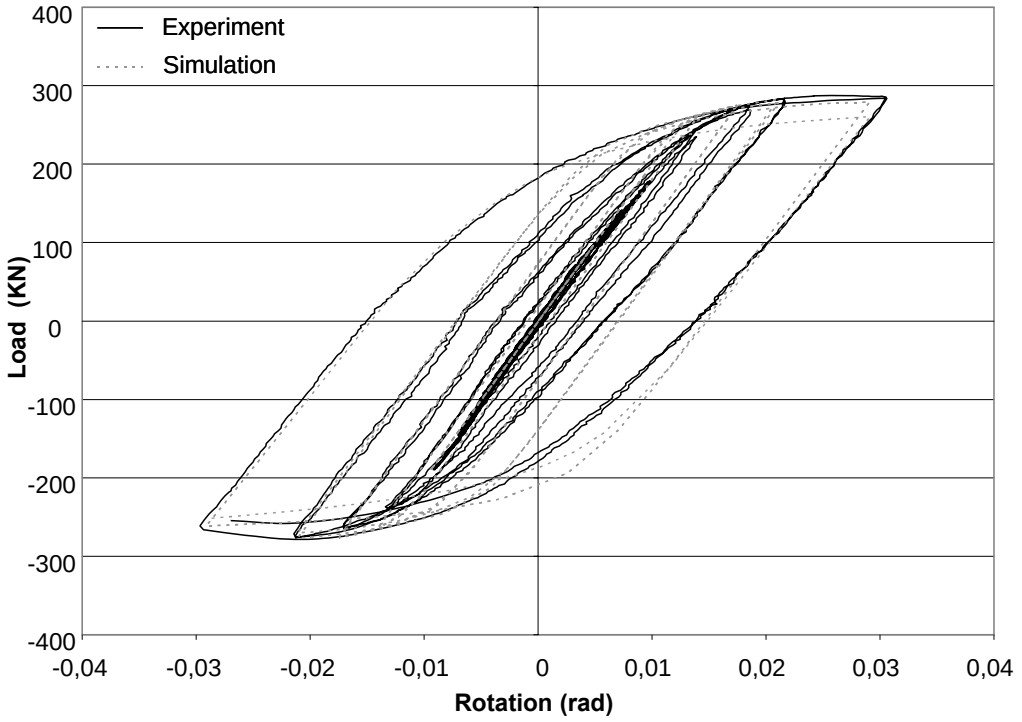

Figure 3.6 Load-Rotation Behavior of HE400AA Beam and Finite Element Simulation

3.6 Sections used in the FEA Study

3.6.1 Introduction

The steel I-sections considered in the study consisted of beam sections with flange slenderness ratios that exceed the flange slenderness limit set forth in current seismic design specifications. In AISC (2005a) limiting slenderness ratios for flanges and webs of rolled or built-up I shaped sections in flexural compression are 7.2 and 59, respectively, for SMF with Fy = 345 MPa and E = 200 GPa. As previously explained beam sections with a welded haunch at the beam bottom was investigated. The sections used for beam types will be presented in this section.

3.6.2 Sections with a Triangular Welded Haunch at the Bottom Flange

Figure 3.47 shows the European and US wide flange beams with FSR greater than 7.2. It can be seen in Fig. 9 that the flange and web slenderness ratios (FSR and WSR) of deep beams (2 < depth/width < 3) range between 7.5 – 9.5 and 43 – 57, respectively, and for shallow beams (1 < depth/width < 2) FSR and WSR range between 7.5 – 13.5 and 20 – 48, respectively. Three different beam depth/width (d/b_f) ratios were selected: 2.79, 2.1, and 1.38. The flange width was taken as 265 mm for all sections and the desired d/b_f ratios were obtained by changing the beam depth. Beam depths were 740, 556.5, and 365 mm for d/b_f ratios of 2.79, 2.1, and 1.38, respectively. For all d/b_f ratios three different FSR were investigated: 8, 9, and 10. Since flange and web local buckling are not independent from each other, different WSR were examined for each flange slenderness ratio. For sections with d/b_f = 2.79, 2.1, and 1.38 WSR of 40-45-50-55-60, 40-45-50, and 30-35-40 were selected, respectively. The desired FSR and WSR values were obtained by changing the flange and web thicknesses of the beams. The geometric properties of the beams modeled in this study are presented in Table 3.1. The depth and length of the triangular haunches were taken as 228/380, 167/278 and 114/190 mm for d/b_f = 2.79, 2.10, and 1.38, respectively. The triangular haunch dimensions were obtained following the guidelines presented in AISC (1999).

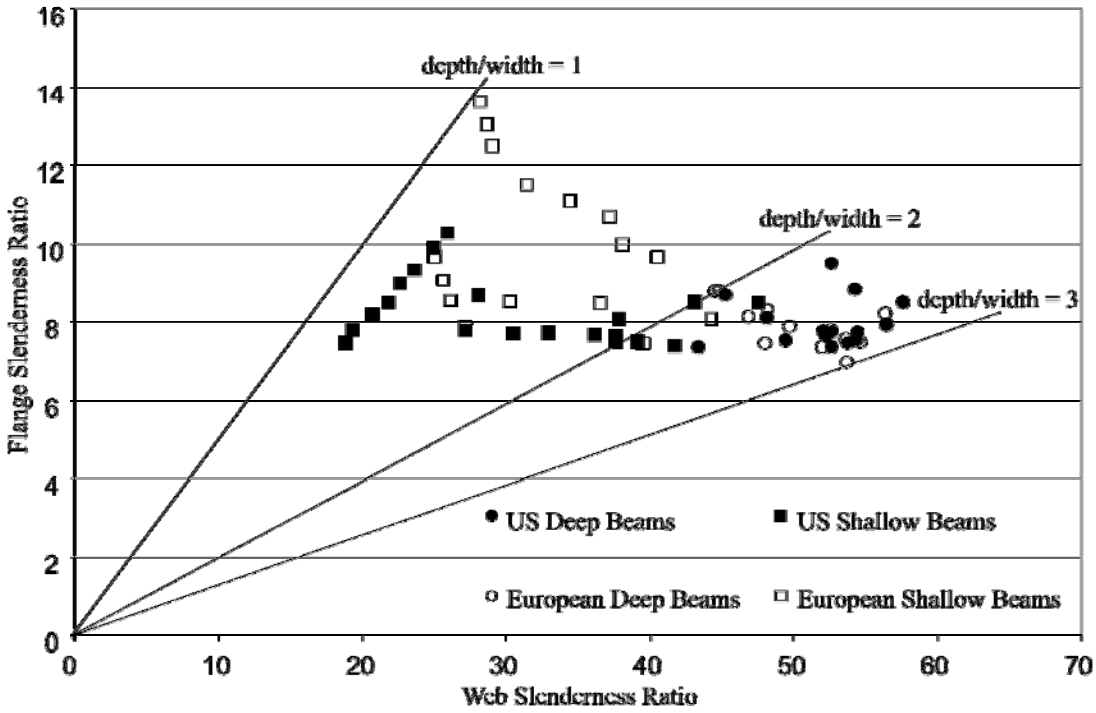

Figure 3.7 US and European Wide Flange Beams with FSR Greater than 7.2

Table 3.1 Geometric Properties of Beam Sections Used in the FEA Study

Section Designation	Beam Length (mm)	Beam Depth (mm)	Flange Width (mm)	Flange Thickness (mm)	Web Thickness (mm)	Depth/Width Ratio
D740-F8W40	3500	740	265	16.56	18.50	2.79
D740-F8W45	3500	740	265	16.56	16.44	2.79
D740-F8W50	3500	740	265	16.56	14.80	2.79
D740-F8W55	3500	740	265	16.56	13.45	2.79
D740-F8W60	3500	740	265	16.56	12.33	2.79
D740-F9W40	3500	740	265	14.72	18.50	2.79
D740-F9W45	3500	740	265	14.72	16.44	2.79
D740-F9W50	3500	740	265	14.72	14.80	2.79
D740-F9W55	3500	740	265	14.72	13.45	2.79
D740-F9W60	3500	740	265	14.72	12.33	2.79
D740-F10W40	3500	740	265	13.25	18.50	2.79
D740-F10W45	3500	740	265	13.25	16.44	2.79
D740-F10W50	3500	740	265	13.25	14.80	2.79
D740-F10W55	3500	740	265	13.25	13.45	2.79
D740-F10W60	3500	740	265	13.25	12.33	2.79
D556-F8W40	3500	556	265	16.56	13.90	2.10
D556-F8W45	3500	556	265	16.56	12.36	2.10
D556-F8W50	3500	556	265	16.56	11.12	2.10
D556-F9W40	3500	556	265	14.72	13.90	2.10
D556-F9W45	3500	556	265	14.72	12.36	2.10
D556-F9W50	3500	556	265	14.72	11.12	2.10
D556-F10W40	3500	556	265	13.25	13.90	2.10
D556-F10W45	3500	556	265	13.25	12.36	2.10
D556-F10W50	3500	556	265	13.25	11.12	2.10
D365-F8W30	3500	380	265	16.56	12.66	1.43
D365-F8W35	3500	380	265	16.56	10.86	1.43
D365-F8W40	3500	380	265	16.56	9.50	1.43
D365-F9W30	3500	380	265	14.72	12.66	1.43
D365-F9W35	3500	380	265	14.72	10.86	1.43
D365-F9W40	3500	380	265	14.72	9.50	1.43
D365-F10W30	3500	380	265	13.25	12.66	1.43
D365-F10W35	3500	380	265	13.25	10.86	1.43
D365-F10W40	3500	380	265	13.25	9.50	1.43

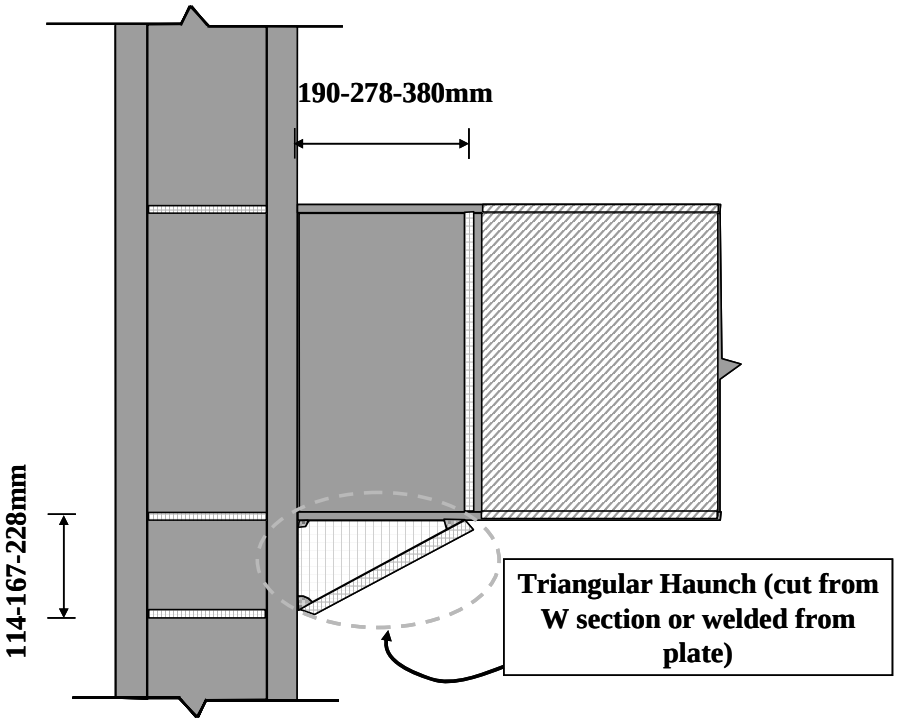

Figure 3.8 Geometric Properties of the Welded Haunch

CHAPTER 4

FEA RESULTS

4.1 Introduction

The results from finite element analyses conducted on the sections described in the Chapter 3 will be presented in this chapter. Some criterias that were used in the evaluation of the behavior of GFRP strengthened steel beam will be presented first, followed by the determination of the optimum width, length, and location of GFRP strips. Results from all the sections will then be given.

4.2 Criterias used in the Evaluation of the Cyclic Behavior of Beams

4.2.1 Rotation Capacity of GFRP Strengthened Beams

The main purpose of GFRP reinforcing application is the mitigation of plastic local buckles. Steel moment frames that are designed to resist earthquake-induced forces are generally grouped into two catagories: a- intermediate moment frames (IMF), b- special moment frames (SMF). IMFs are designed to withstand an interstory drift angle of 0.02 rad, whereas SMFs are designed to withstand an interstory drift angle of 0.04 rad, without significant strength losses.

The additional rotation capacity provided by the GFRPs will be investigated to determine whether the reinforced beams can be used in areas where IMF or SMF designs are mandatory. In the results it is assumed that the GFRP loses contact with the steel flanges once local buckling occurs. Therefore, the analyses of beams with GFRP

reinforcement were conducted up to the rotation levels that would initiate local buckling.

4.2.2 Maximum Design Capacity of the Beams

In AISC (2005a) the maximum design capacity of a beam-column connection is given by the following equation:

$$M_{pr} = C_{pr} R_y F_y Z_e \qquad AISC\ 2005a \tag{4.1}$$

where:

C_{pr} = coefficient for strain hardening

$$C_{pr} = \frac{F_y + F_u}{2F_y} \le 1.2 \qquad (ANSI / AISC 358-05 Equation 2.4.3-2) \tag{4.2}$$

F_y = specified minimum yield strength of the type of steel used (MPa)

F_u = specified minimum tensile strength of the type of steel used (MPa)

R_y = ratio of the expected yield stress to the specified minimum yield stress (AISC 2005b, Table I-6-1)

$F_y Z_e$ = M_p = Plastic Moment of the beam section

As explained in Chapter 3 bilinear kinematic strain hardening model is adopted in the FEA study. The secondary stiffness is taken as 1/100 of the elastic modulus after the yield stress. The C_{pr} coefficient is taken as 1.2 in this study by accepting that rupture occurs at an elongation of 10% (common for many steels). For most steel types R_y is taken as 1.1 (AISC 2005a), however for the analytical study R_y is taken as 1.0. Therefore:

$$\frac{M_{pr}}{M_p} = 1.2 \tag{4.3}$$

It is obvious that adding GFRP to the beam flanges will increase the moment capacity of the beam section. However, this capacity increase should be less than 1.2, because in this study it is assumed that the connections are designed 20% over their plastic capacity. The finite element results were checked whether the capacity increase was more than 20% or not.

4.2.3 Shear Stresses Checked

The sections listed in Table 3.1 were analyzed both with and without GFRP strips in order to observe the effects of GFRP strips to the cyclic behavior of each beam section. In evaluating the cyclic behavior of sections reinforced with GFRP strips the moment at the column face, shear stress of the interface between steel and GFRP, and interlaminar shear stress of GFRP strips were checked at every load step prior to local buckling to make sure the design moment of the connection, shear strength of the interface, and interlaminar shear strength of the GFRP strips were not exceeded. The maximum design moment of the connection was taken as 1.2Mp, which is in correlation with AISC (2005c).

There are many potential failure modes of a steel-FRP composite system under flexure. The major ones that involve the FRP material and the adhesive layer are tensile rupture or compressive failure of the FRP material and debonding of the steel-FRP bond surface. Among these failure modes, debonding is often the weakest link (Cadei et al. 2004). The most significant stresses in a bond layer between steel and FRP are the longitudinal shear stresses and through the thickness normal stresses, which is also known as peeling stress. These stresses are generally the highest at the ends of the FRP laminates or in the regions of large local deformations such as buckling. A tensile normal stress at the adhesive layer may lead to peeling of the FRP away from the steel surface and accelerate debonding. However, the negative effects of the peeling stresses are neglected in this study and focus is mainly given to the longitudinal shear stresses.

Recently, many studies have been conducted that investigated potential ways to mitigate peeling stresses and premature debonding. Some of the recommended applications of these research investigations include reverse tapering the edges of the FRP laminates (Schnerch et al. 2007) and providing cross-wraps (Chen and Das 2009). In addition, Cadei et al. (2004) showed that for system with FRP laminates of small

thickness, which is the case in this study, the peeling stresses were negligible compared with shear stresses. Nevertheless, it is assumed in this study that the ends of the FRP material are anchored to the steel surface in some way and that peeling stresses do not affect debonding. Furthermore, the increase in peeling stresses in the buckled regions is not of interest in this research. It is further assumed that the steel-GFRP composite action ends when either of the following takes place: a- local buckling initiates; b- interfacial shear strength of the steel-GFRP bond layer is exceeded prior to local buckling; or c- interlaminar shear strength of the GFRP laminates is exceeded prior to local buckling. The tensile and compressive stresses that developed on the GFRP strips were much lower than the measured tensile and compressive strengths of the GFRP material and therefore were not discussed in the results.

In order to determine the interfacial and interlaminar shear strength values that would be used in the study, a literature review was conducted. It was seen that the interfacial shear strength of steel-GFRP surfaces bonded with commonly used epoxies could reach up to 20-25 MPa (El Damatty and Abushagur 2003, Boone 2002) and the interlaminar shear strength of commonly used GFRP materials could reach up to 20 MPa (Lili, et al. 2008). A resistance factor of 0.75 was applied to the lower limit of the above interfacial shear strengths and a resistance factor of 0.90 was applied to the above interlaminar shear strength. Hence, shear strength of the interface and interlaminar shear strength of the GFRP strips were taken as 15.0 MPa and 18.0 MPa, respectively. A lower resistance factor was accepted for the interfacial shear strength as compared to that for the interlaminar shear strength. This was due to the fact that bonding GFRP strips to steel surfaces involves many steps that need to be performed carefully and could be difficult to control out in the field.

4.3 FEA Results

4.3.1 Introduction

The analyses results are evaluated from the M/M_p-Θ (Normalized moment at column face – rotation) behavior of each section. The yield strength of steel is taken as

345 MPa, as previously explained. AISC (2005a) requires the normalized moment to be calculated at the column face. The determination of optimum width, length, and location of GFRP strips will be presented first, followed by the results.

4.3.2 Determination of Optimum Width, Length, and Location of GFRP Strips

In order to determine the optimum location, length, and width of GFRP strips a series of analyses were conducted with a beam section having a depth/width ratio of 2.79, depth of 740 mm, width of 265 mm, FSR of 10, and WSR of 65. Although this section (D740-F10W65) is not among the sections listed in Table 3.1, the response of the sections listed in Table 3.1 to different GFRP length, width, thickness, and placement configurations were similar to that of section D740-F10W65. Three different configurations were considered for GFRP placement: 1- Bottom of top flange and top of bottom flange outside the welded haunch region (Figure 4.1), 2- Both sides of top and bottom flanges outside the welded haunch region (Figure 4.2), and 3- Both sides of top flange at outside and inside the welded haunch region and both sides of bottom flange only at outside of the welded haunch region (Figure 4.3). As seen in these figures the length, width, and thickness of GFRP strips are identified as ratios of beam depth, beam width, and flange thickness, respectively. The length of GFRP strips denotes the length beyond the welded haunch stiffener in the plastic hinge region of the beam. The results obtained from several analyses with different GFRP widths, lengths, and locations are presented in Table 4.1.

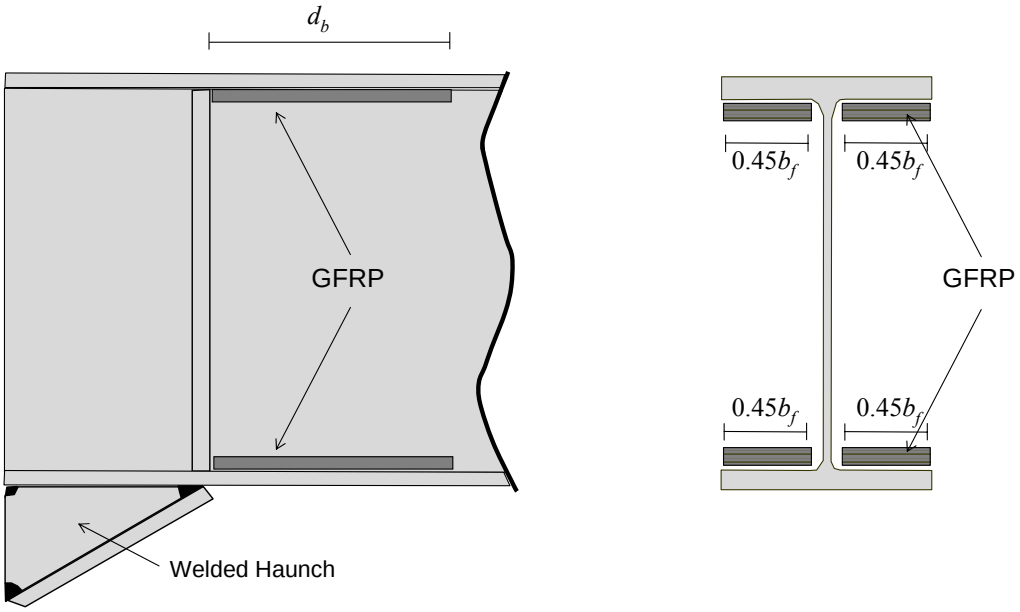

Figure 4.1 GFRP Placement: Configuration 1

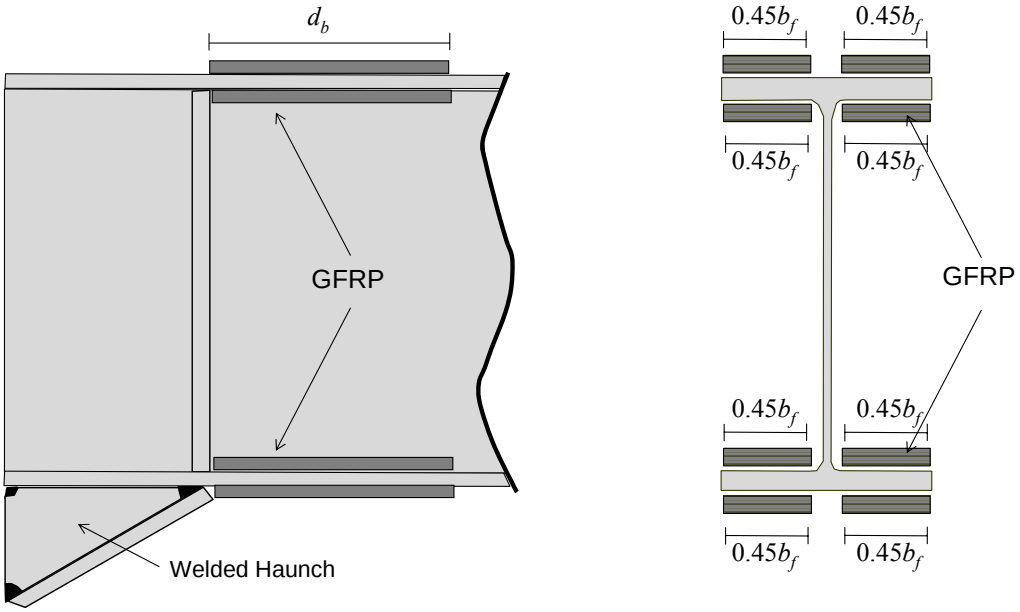

Figure 4.2 GFRP Placement: Configuration 2

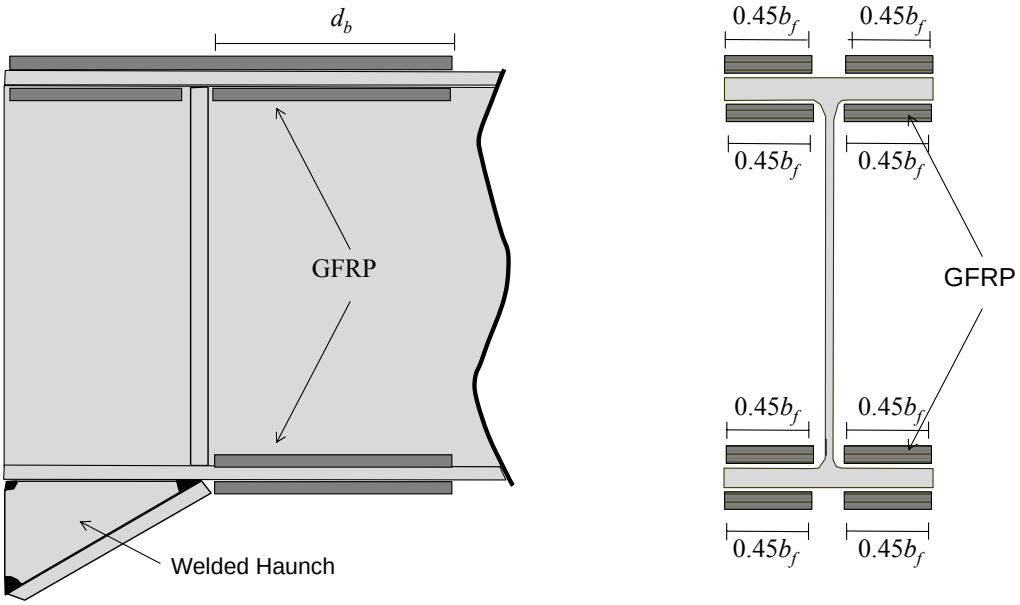

Figure 4.3 GFRP Placement: Configuration 3

Table 4.1 Analyses Results for Section D740-F10W65

GFRP Placement	# of Layers (Total thickness of GFRP)	t_{GFRP}	L_{GFRP}	b_{GFRP}	Negative Bending			Positive Bending			@ 0.01 rad of Rotation		@ Last Rotation/Cycle Prior to Local Buckling	
					M_{max}/M_p	Last Rot./Cycle Prior to Local Buckling	Location of Local Buckling (outside or inside of WH region)	M_{max}/M_p	Last Rot./Cycle Prior to Local Buckling	Location of Local Buckling (outside or inside of WH region)	Max Interfacial Shear Stress (MPa)	Max Interlaminar Shear Stress (MPa)	Max Interfacial Shear Stress (MPa)	Max Interlaminar Shear Stress (MPa)
Bare	-	-	-	-	0.89	$0.010/2^{nd}$	Outside	0.95	$0.015/1^{st}$	Outside	-	-	-	-
Configuration 1 (Fig. 4.1)	6 (5.4 mm)	$0.41t_f$	L_b	$0.20b_f$	0.90	$0.010/2^{nd}$	Outside	0.96	$0.015/2^{nd}$	Outside	11.5	12.5	19.7	19.3
			$2d_b$	$0.20b_f$	0.90	$0.010/2^{nd}$	Outside	0.96	$0.015/2^{nd}$	Outside	11.5	12.5	19.7	19.3
			$2d_b$	$0.45b_f$	0.93	$0.015/1^{st}$	Outside	0.97	$0.015/2^{nd}$	Outside	9.7	11.4	16.5	17.6
Configuration 2 (Fig. 4.2)	3+3 (5.4 mm)	$0.41t_f$	$2d_b$	$0.45b_f$	0.94	$0.015/1^{st}$	Outside	0.97	$0.015/2^{nd}$	Outside	5.4	8.1	8.7	12.4
	3+3 (5.4 mm)	$0.41t_f$	d_b	$0.45b_f$	0.94	$0.015/1^{st}$	Outside	0.97	$0.015/2^{nd}$	Outside	5.4	8.1	8.7	12.4
	4+4 (7.2 mm)	$0.54t_f$	d_b	$0.45b_f$	0.94	$0.015/1^{st}$	Outside	0.97	$0.015/2^{nd}$	Inside	6.9	9.2	11.6	14.3
	5+5 (9.0 mm)	$0.68t_f$	d_b	$0.45b_f$	0.94	$0.015/2^{nd}$	Outside	0.98	$0.015/2^{nd}$	Inside	8.3	10.2	14.3	16.2
Configuration 3 (Fig. 4.3)	4+4 (7.2 mm)	$0.41t_f$	d_b	$0.45b_f$	0.94	$0.015/1^{st}$	Outside	0.98	$0.015/2^{nd}$	Outside	6.8	9.2	12.6	14.1

Prior to looking at Table 4.1, the M/M_p-Θ (normalized moment at column face – rotation at fixed end) behavior of a beam with and without GFRP will be investigated to clarify how the values presented in Table 4.1 were obtained. Figure 4.4 shows the M/M_p-Θ behaviors of a bare beam and beam with GFRP. depth and width of the beam were 740mm and 265 mm, respectively. In addition, the beam d/b_f ratio, FSR, and WSR were 2.79, 9, and 55, respectively. The GFRP configuration was identical to the one shown in Figure 4.3. The GFRP length, thickness, and width were d_b, where d_b is equal to depth of the beam, $0.37t_f$ (3 layers at top and 3 layers at bottom of each flange = 3 + 3 layers), where t_f is equal to thickness of the flange, and $0.45b_f$, where b_f is equal to the flange width. In the figure positive rotation (bending) corresponds to compression at the top flange and negative rotation (bending) corresponds to compression at the bottom flange. It can be observed from the figure that for the bare beam the last cycles prior to local buckling were 1st cycle of 0.015 rad of rotation and 1st cycle of 0.017 rad of rotation at bottom and top flanges, respectively. In other words, local flange buckling occurred at 2nd cycle of 0.015 rad of rotation and 1st cycle of 0.02 rad of rotation at bottom and top flanges, respectively. The fact that local buckling initiates at bottom flange prior to top flange is consistent with the applied initial imperfections. For the beam with GFRP the last cycles prior to local buckling were 2nd cycle of 0.015 rad of rotation and 1st cycle of 0.02 rad of rotations at bottom and top flanges, respectively. The maximum shear stress at the interface and interlaminar shear stress at these cycles were 13.4 and 15.0 MPa, respectively. The maximum interfacial shear stress was very close to the accepted interfacial shear strength of the bond surface between steel and GFRP. The maximum M/M_p values were 0.99 and 1.08 for the beam with GFRP for negative and positive bendings, respectively; which were lower than the design moment of the connection. The addition of GFRP to the steel section enabled the rotation capacities in positive and negative bendings to increase by 1 cycle, whereas the increase in the moment capacity was minimal. Local distortions in the bottom flange observed in the model with GFRP at a rotation of 0.02 rad are shown in Figure 4.5. As can be seen from the figure major distortions occur in the flanges with some kinking at the web adjacent to the distorted flange.

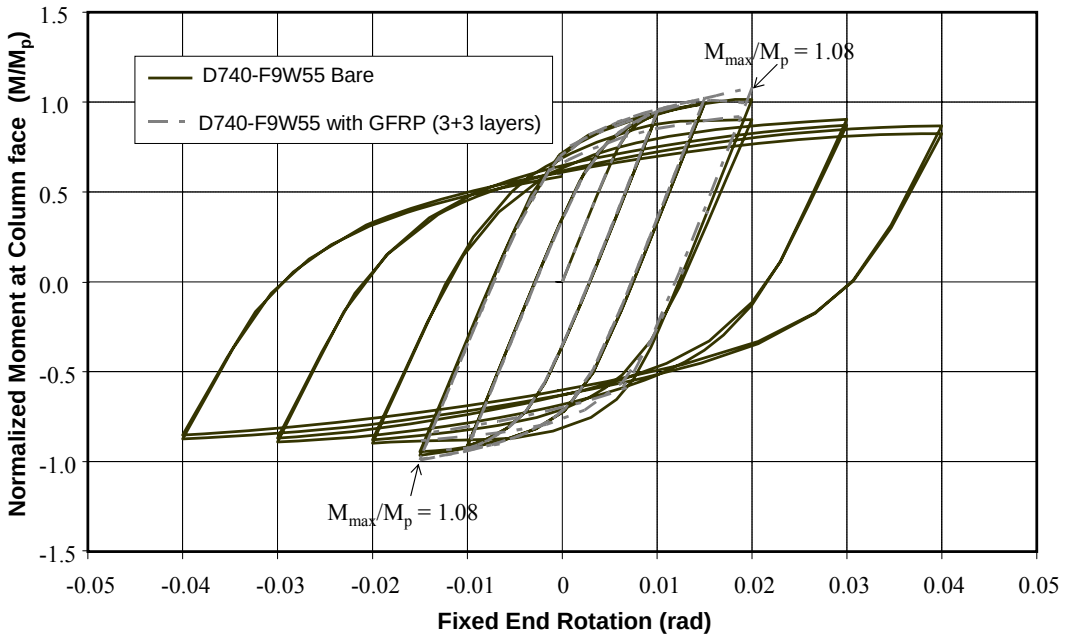

Figure 4.4 M/M_p-Θ relationships of D740-F9W55 section with and without GFRP

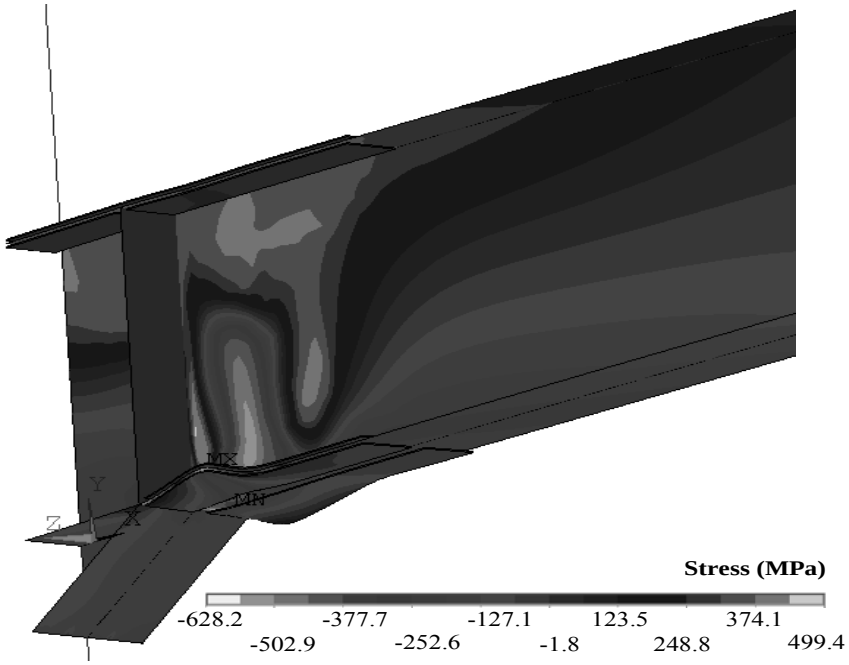

Figure 4.5 Local flange buckling observed in bottom flange at 1st cycle of 0.02 rad of rotation for D740-F9W55

Table 4.1 presents results from a series of finite element analyses conducted with a 740 mm deep and 265 mm wide beam section. The depth/width ratio, FSR, and WSR of the section were 2.79, 10, and 65, respectively. The effects of different GFRP length (L_{GFRP}), width (w_{GFRP}), thickness (t_{GFRP}), and placement configurations (Figure 4.1, 4.2, or 4.3) to the overall cyclic behavior of the beam section were examined. The first column indicates the placement configuration of GFRP strips. In the 2nd, 3rd, 4th, and 5th columns layer number (6 layers imply GFRP placed on one side of the flanges as shown in Figure 4.1, 3+3 layers imply GFRP is placed on top and bottom of both flanges as shown in Figure 4.2 or Figure 4.3), thickness of GFRP (as a ratio of flange thickness, t_f), length of GFRP (as a ratio of beam depth d_b beyond the haunch stiffener), and width of GFRP (as a ratio of flange width, b_f, for each side of a flange) are presented, respectively. The 6th and 9th columns present M_{max}/M_p values for negative and positive bendings, respectively. The 7th and 10th columns present the last rotation/cycle number achieved prior to local buckling for negative and positive bendings, respectively. The 8th and 11th columns indicate whether buckling occurs inside or outside of the welded haunch region at the flanges. The 12th and 13th columns give the maximum interfacial shear stress at the surface between steel and GFRP and interlaminar shear stresses in GFRP at the 2nd cycle of 0.01 rad of rotation, respectively. These values are the higher of stress values that develop at the top and bottom flanges at this rotation. The purpose of presenting these values is to compare the shear stresses of different GFRP systems at a fixed rotation prior to local buckling. In the 14th and 15th columns the maximum interfacial and interlaminar shear stresses are presented at the last rotation/cycle prior to local buckling, which are presented in columns 7 and 10, for negative and positive bendings, respectively. The maximum interfacial and interlaminar shear stresses occurred around the welded haunch stiffener. The values presented in columns 14 and 15 are the shear stress values that develop at the last rotation/cycle of the bottom flange. Due to the implemented imperfections top flange buckled at a later rotation/cycle than the bottom flange. However, the maximum interfacial and interlaminar shear stress values for the top flange at the corresponding last rotation/cycle prior to local buckling were similar to the values given in columns 14 and 15.

The first row of Table 4.1 contains information about the bare steel model. The 2nd, 3rd, and 4th rows are for steel-GFRP systems with 6 layers of GFRP (Figure 4.1 with

t_{GFRP} = 0.40t_f). The 5th and 6th rows are for systems with 3 layers of GFRP (Figure 4.2 with t_{GFRP} = 0.20t_f +0.20t_f = 0.40t_f) on each side of the flanges (3+3 layers). The total thickness of the GFRP strips in one flange for 6 layers and 3+3 layers are identical. However, in 6 layer systems a thicker GFRP is placed on one side of the flanges, whereas in 3+3 layer systems a thinner GFRP is placed on both sides of the flanges. Comparing rows 2 and 3 indicate that keeping the length of GFRP laminates at twice the beam depth beyond the welded haunch stiffener is identical to using full length GFRP laminates. For both of the systems maximum moments at column face, last rotation/cycle numbers, location of local buckling, maximum interfacial and interlaminar shear stresses at 0.01 rad of rotation, and maximum interfacial and interlaminar shear stresses at last cycle prior to local buckling are identical. In row 4 results from a steel-GFRP system with a GFRP length, thickness, and width of 2d_b, 0.40t_f, and 0.45b_f, respectively, are presented. Increasing the width of the GFRP strips to 0.45b_f from 0.20b_f decreased the maximum interfacial and interlaminar shear stresses at 0.01 rad of rotation to 9.7 and 11.4 MPa from 11.5 and 12.5 MPa, respectively. An increase in the last rotation/cycle number prior to local buckling was observed only in negative bending. The last rotation/cycle number prior to local buckling at negative bending for the system with a GFRP width of 0.20b_f was 2nd cycle of 0.01 rad of rotation; whereas for the system with GFRP width of 0.45b_f this value increased to 1st cycle of 0.015 rad of rotation. In order to further decrease the interfacial and interlaminar shear stresses, a system with GFRP placed on both sides of flanges were analyzed (rows 5 and 6), keeping the total thickness of GFRP the same. It was seen that using GFRP strips on both sides of flanges (Figure 4.2) decreased the maximum interfacial and interlaminar shear stresses at 0.01 rad of rotation to 5.4 and 8.1 MPa from 9.7 and 11.4 MPa (row 4), respectively. Another analysis was conducted to determine whether the length of the GFRP strips could further be decreased. Row 6 presents results from a system identical to the system in row 5, except the length of the GFRP strips. Comparing the results presented in rows 6 and 5 indicate that decreasing the length of GFRP strips to d_b from 2d_b does not weaken the contribution of GFRP strips. For the system presented in row 6 the maximum interfacial and interlaminar shear stresses at last cycle prior to local buckling were 8.7 and 12.4 MPa, respectively. Since these values were smaller than the accepted interfacial and interlaminar shear

stresses (13.5 and 18 MPa), the analyses were continued by increasing the layer number of GFRP.

Rows 7 and 8 present results from steel-GFRP systems with 4+4 and 5+5 layers of GFRP, bringing the total thickness of GFRP to $0.54t_f$ and $0.68t_f$, respectively. The response of the system with 4+4 layers of GFRP did not differ from that of the system with 3+3 layers of GFRP, except the maximum interfacial and interlaminar shear stresses and the location of initial flange buckling at the top flange. The maximum interfacial and interlaminar shear stresses at the last step prior to local buckling for the 4+4 layered system was 11.6 and 14.3 MPa compared to 8.7 and 12.4 MPa for the 3+3 layered system, respectively. Another difference was observed in the location of the top flange local buckling. In the system with 3+3 layers of GFRP initial top flange buckling was observed just outside the welded haunch (WH) region. However, in the system with 4+4 layers of GFRP initial top flange local buckling was observed inside the WH region adjacent to the column face. The presence of the welded haunch at the bottom flange prevents bottom flange local buckling to shift adjacent to the column face inside the WH region. Since the interfacial or interlaminar shear strengths were not exceeded in the 4+4 layered system, the thickness of the GFRP was increased to 5+5 layers and another analysis was conducted. Increasing the number of layers to 5+5 improved the rotation capacity of the bottom flange prior to local flange buckling by 1 cycle, bringing it to 2nd cycle of 0.015 rad of rotation. However, the interfacial shear strength was exceeded in this system. The location of top flange local buckling was again in the WH region adjacent to the column face. Since local flange buckling adjacent to the column face is not desirable, another analysis was conducted by providing additional GFRP at both sides of the top flange inside the WH region as shown in Figure 4.3 in an effort to move the top flange buckling back to the plastic hinge region just outside the welded haunch region. Row 9 presents results from a system with 4+4 layers of GFRP and GFRP configuration identical to the one shown in Figure 4.3. The addition of the GFRP inside the welded haunch region did not have an effect on the rotation capacities prior to local buckling as compared to the behavior obtained from the system presented in row 7. However, the initiation of local buckling at the top flange was moved back to the plastic hinge region adjacent to the WH stiffener.

The results presented in Table 4.1 revealed that the contribution of GFRP strips to the cyclic behavior of steel beams modified by a welded haunch at bottom flange was

limited by the interfacial shear strength of the bonded surface between steel and GFRP. The optimum length and width of GFRP strips, which lead to the smallest interfacial and interlaminar shear stresses, were d_b and $0.45b_f$, respectively, and the optimum GFRP configuration was configuration 3 (Figure 4.3).

Prior to conducting finite element analyses with the sections listed in Table 3.1, the effects of modulus of elasticity of GFRP and placing GFRP on the web to the cyclic behavior of beams are investigated as well, Table 4.2 presents results from analyses conducted on steel-GFRP systems with higher GFRP elastic modulus and different GFRP configurations. Rows 1 and 2 of Table 4.2 present results from the bare steel section and steel-GFRP system with GFRP configuration 3 (Figure 4.3) and 4+4 number of GFRP layers. The system in row 2 is the same system presented in row 9 of Table 4.1. The systems in rows 3 and 4 are identical to the system in row 2, except the elastic modulus of GFRP. The elastic modulus of GFRP was taken as 20000 and 200000 MPa for the systems in rows 3 and 4, respectively; whereas the elastic modulus of GFRP was taken as 10000 MPa for the system presented in row 2. Finally in rows 5 and 6, results from a steel-GFRP steel system with GFRP (elastic modulus of 10000 MPa) placed also in the web are presented. Results presented in row 5 are for a steel GFRP system in which GFRP is also placed in the web outside the WH region for a distance d_b, in addition to the GFRP configuration shown in Figure 4.3. Results from the system with GFRP placed in the web both inside and outside the WH region in addition to the GFRP configuration shown in Figure 4.3 are presented in row 6.

Table 4.2 Analyses Results for Section D740-F10W65

	1	2	3	4	5	6	7	8	9	10	11	12	13	14	15
								Negative Bending			Positive Bending			@ Last Rotation/Cycle Prior to Local Buckling	
	GFRP Placement	# of Layers (Total thickness of GFRP)	GFRP Placement on Web	E of GFRP (MPa)	t_{GFRP}	L_{GFRP}	b_{GFRP}	M_{max}/M_p	Last Rot./Cycle Prior to Local Buckling	Location of Local Buckling (outside or inside of WH region)	M_{max}/M_p	Last Rot./Cycle Prior to Local Buckling	Location of Local Buckling (outside or inside of WH region)	Max Interfacial Shear Stress (MPa)	Max Interlaminar Shear Stress (MPa)
1	Bare	-	-	-	-	-	-	0.89	0.010/2nd	Outside	0.95	0.015/1st	Outside	-	-
2	Configuration 3 (Figure 4.3)	4+4 (7.2 mm)	N/A	10000	$0.54t_f$	d_b	$0.45b_f$	0.94	0.015/1st	Outside	0.98	0.015/2nd	Outside	12.6	14.1
3			N/A	20000	$0.54t_f$	d_b	$0.45b_f$	0.99	0.017/1st	Outside	1.01	0.018/1st	Outside	19.6	24.2
4			N/A	200000	$0.54t_f$	d_b	$0.45b_f$	1.18	0.017/1st	Outside	1.22	0.018/1st	Outside	59.9	78.4
5	Configuration 3 (Figure 4.3)	4+4 (7.2 mm)	Out of the WH region	10000	$0.54t_f$	d_b	$0.45b_f$	0.96	0.015/1st	Outside	1.00	0.015/2nd	Inside	12.9	14.5
6			Inside and outside of the WH region	10000	$0.54t_f$	d_b	$0.45b_f$	0.97	0.015/1st	Outside	1.00	0.015/2nd	Outside	12.8	14.3

Comparing the results presented in rows 2, 3, and 4 revealed that increasing the elastic modulus of GFRP had a minor effect on the rotation capacities prior to local buckling for both top and bottom flanges. For both systems with higher elastic modulus (20000 and 200000 MPa) the last step prior to local buckling increased to 1st cycle of 0.017 rad of rotation and 1st cycle of 0.018 rad of rotation as compared to 1st cycle of 0.015 rad of rotation and 2nd cycle of 0.015 rad of rotation for the system with elastic modulus of 10000 MPa for bottom and top flanges, respectively. However, the maximum interfacial and interlaminar shear stresses for both systems prior to local flange buckling increased beyond the accepted shear strengths. For the system with GFRP modulus of 20000 MPa interfacial and interlaminar shear stresses were 19.6 and 24.2 MPa at the end of 2nd cycle of 0.015 rad of rotation. For the system with GFRP modulus of 200000 MPa not only the maximum shear stresses but also the maximum moment at the column face increased considerably. The maximum interfacial and interlaminar shear stresses were 59.9 and 78.4 MPa, respectively, at the end of 2nd cycle of 0.015 rad of rotation. The maximum normalized column moments (M_{max}/M_p) were 1.18 and 1.22 for negative and positive bendings, respectively, exceeding the design moment capacity of the connection. The addition of GFRP on the web also did not have a major effect on the behavior (rows 5 and 6). The maximum column face moments and shear stresses at the last rotation prior to local buckling increased slightly for both configurations. The addition of GFRP on the web only at the outside of the welded haunch region (row 5) forced the location of initial local buckling to move back to the top flange inside the welded haunch region. The reason for such behavior is probably due to the fact that the addition of the GFRP on the web prevents the initiation of local buckling outside the welded haunch region and forces it to initiate inside the welded haunch region where the web is free of GFRP. Addition of GFRP to the web inside the welded haunch region moves local buckling back to the plastic hinge region beyond the welded haunch stiffener at the flanges (row 6).

4.3.3 Results

4.3.3.1 Sections with Depth/Width Ratio of 2.79

The sections presented in Table 3.1 were analyzed with the GFRP configuration shown in Figure 4.3. The width of GFRP was taken as $0.45b_f$ and the length as d_b beyond the haunch stiffener for all sections. Results from analyses conducted on sections with a depth/width ratio of 2.79 will be presented in this section. Prior to looking at the results in a table format the M/M_p-Θ behavior of one of the sections will be presented. The normalized moment at the column face – rotation at fixed end (M/M_p-Θ) behavior of section D740-F8W40 with and without GFRP is shown in Figure 4.6. Three layers of GFRP on each side of the flanges were used, bringing the total thickness of the GFRP to 5.4 mm or $0.33t_f$. In the figure positive and negative rotations indicate compression on top and bottom flanges, respectively. It can be observed from the figure that in the bare section strength degradation initiates at the end of the 2nd cycle of 0.02 rad of rotation and 1st cycle of 0.02 rad of rotation for positive and negative bendings, respectively. The strength degradations continue in the following rotations as the severity of local buckling increases and the normalized column moments at the column face at the end of the 2nd cycle of 0.04 rad of rotation drop to 0.90 and 0.94 for positive and negative bendings, respectively. These values are higher than the minimum required flexural resistance at the column face ($0.80M/M_p$) at an interstory drift angle of 0.04 rad for special moment frames as stated in AISC (2005a). The addition of 3+3 layers of GFRP to the steel section increases the rotation/cycle values prior to local buckling. For positive and negative bendings these values increase to 1st cycle of 0.025 rad of rotation and 2nd cycle of 0.02 rad of rotation, respectively. Although there seems to be no strength degradation until the end of 1st cycle of 0.03 rad of rotation for both positive and negative bendings, investigating the stress fields available in ANSYS (2007) revealed that local flange buckling initiated at the end of the above-mentioned rotations/cycles. The analysis of the section with GFRP was stopped at the end of 0.03 rad of rotation since the maximum interfacial and interlaminar shear strengths were previously exceeded. The maximum normalized moments at the column face (M_{max}/M_p) were 1.09 and 1.20 for negative and positive

bendings, respectively, which were smaller or equal to the design moment of the connection. It can be observed in Figure 4.6 that these values were actually achieved at the end of the 1st cycle of 0.03 rad of rotation, at which maximum interfacial shear strength was already exceeded. Thus, contribution of the GFRP was neglected after the 1st cycle of 0.025 rad of rotation in which maximum interfacial shear strength was exceeded.

The normalized moment at the column face – rotation at fixed end (M/M_p-Θ) behavior of sections with depth/width ratio of 2.79 listed in Table 3.1 was examined. Table 4.3 presents the key results obtained from the M/M_p-Θ behaviors of these sections. Columns 1, 2, and 3 indicate the section designation, number of layers and total thickness of GFRP in mm, and thickness of GFRP as a ratio of the thickness of the flange, respectively. The GFRP layer number and thickness presented in columns 2 and 3 are the thickest GFRP that could be used without exceeding the interfacial shear strength of the bond surface between steel and GFRP or interlaminar shear strength of GFRP laminates prior to local flange buckling. Interfacial and interlaminar shear stresses increased significantly once flange local buckling initiated. Therefore, the contribution of GFRP strips could be best observed by looking at the rotation values achieved prior to flange local buckling without exceeding the interfacial and interlaminar shear strengths. The 4th and 6th columns present last rotation/cycle of bare sections prior to local buckling for negative and positive bendings, respectively. The 5th and 7th columns present the last rotation/cycle number of sections with GFRP prior to local buckling for negative and positive bendings, respectively. The 8th and 9th columns present M_{max}/M_p values of sections with GFRP for negative and positive bendings, respectively. The 10th and 11th columns present M/M_p values of bare sections at the end of the 2nd cycle of 0.04 rad of rotation for negative and positive bendings, respectively. The maximum interfacial and interlaminar shear stresses of sections with GFRP at the last rotation/cycle prior to local are presented in columns 8 and 9 for negative and positive bendings, respectively. Maximum shear stresses generally occurred around the welded haunch stiffener for both flanges.

It can be seen from columns 2 and 3 for almost all of the sections 3+3 number of GFRP layers were the most that can be used without exceeding the interfacial shear strength of the bond surface between steel and GFRP prior to local buckling. Only section D740-F8W60 required 2+2 number of layers in order not to exceed the

interfacial shear strength prior to flange local buckling. The interfacial shear stresses achieved for the sections prior to local flange buckling ranged between 11.9 to 13.4 MPa, which were somewhat close to the accepted interfacial shear strength (15.0 MPa) of the bond surface. The interlaminar shear stresses of the sections ranged between 13.1 and 15.0 MPa. The interfacial shear strength of GFRP strips was taken as 18 MPa. Results presented in column 8 and 9 indicate that the design moment capacity of the connection ($1.2M_p$) was not exceeded neither in negative nor positive bending in any of the sections. The largest normalized column face moment occurred in section D740-F8W40 at positive bending with 1.20. Observing the results presented in columns 10 and 11 show that strength degradation in most of the sections was below 20% at the end of the 2nd cycle of 0.04 rad of rotation. Sections D740-F9W60 / F10W45 / F10W50 / F10W55 / F10W60 experienced strength degradations in excess of 20% at the end of the 2nd cycle of 0.04 rad of rotation, especially in positive bending.

For bare sections initial local buckling occurred at a lower rotation/cycle at the bottom flange than the top flange, which was consistent with the implemented imperfections in the models. In negative bending almost none of the bare sections reached 0.02 rad of rotation without local buckling. Only sections D740-F8W40 and D740-F8W45 reached the first cycle of 0.02 rad of rotation without any local buckling. However, in positive bending bare sections D740-F8W40 / F8W45 / F9W40 / F9W45 completed the two cycles of 0.02 rad of rotation and sections D740-F8W50 / F8W55 / F9W50 / F10W40 / F10W45 completed the first cycle of 0.02 rad of rotation without any local buckling. Comparing the rotation values of bare sections with sections with GFRP strips revealed that the addition of 3+3 layers of GFRP increased the rotation capacity of bare sections prior to local buckling by at least one cycle in both negative and positive bendings. The only exception to this was section D740-F10W60 in positive bending, which was the most slender section among all with a depth/width ratio of 2.79. The addition of 3+3 layers of GFRP enabled almost all of the sections to reach to 0.02 rad of rotation in positive bending. Sections D740-F9W60 and D740-F10W60 reached only 0.017 and 0.016 rad of rotations in positive bending, respectively, with the addition of the GFRP strips. In negative bending the addition of 3+3 layers of GFRP strips enabled all of the sections to complete 2 cycles at 0.015 rad of rotation or higher without any local buckling. Sections D740-F8W40 and D740-F8W45 completed the full 2 cycles of 0.02 rad of rotation, section D740-F8W50 completed the first cycle of 0.02

rad of rotation, and section D740-F8W55 completed the first cycle of 0.018 rad of rotation. The rest of the sections completed the second cycle of 0.015 rad of rotation in negative bending without any local buckling.

Examining the rotations in positive bending of sections D740-F8W40 / F8W45 and D740-F9W40 / F9W45 indicates that the contribution of the GFRP strips to the rotation capacity of the sections decreases with increasing FSR. While the rotation capacities in positive bending of bare sections D740-F8W40 / F8W45 and D740-F9W40 / F9W45 with no local buckling were the same (second cycle of 0.02 rad of rotation), the rotation capacities with no local buckling differed with the addition of GFRP strips to these sections. While sections D740-F8W40 / F8W45 with an FSR of 8 were capable of reaching the end of 1st cycle of 0.025 rad of rotation with the addition of the GFRP strips, sections D740-F9W40 / F9W45 with an FSR of 9 reached the end of 1st cycle of 0.023 rad of rotation with the addition of the GFRP strips without any local buckling. The same comment could be maid for the relationship between WSR and contribution of GFRP reinforcement. Comparing the rotation values prior to local buckling of section D740-F8W50 and D740-F8W55 in negative bending indicate that the contribution of GFRP strips decreases as the WSR of the sections increase. The addition of 3+3 layers of GFRP strips to section D740-F8W50 with WSR of 50 increased the rotation capacity of the section to 0.02 rad of rotation from 0.015 rad of rotation. However, for section D740-F8W55 with WSR of 55 the addition of 3+3 layers of GFRP strips increased the rotation capacity of the section to 0.018 rad of rotation from 0.015 rad of rotation.

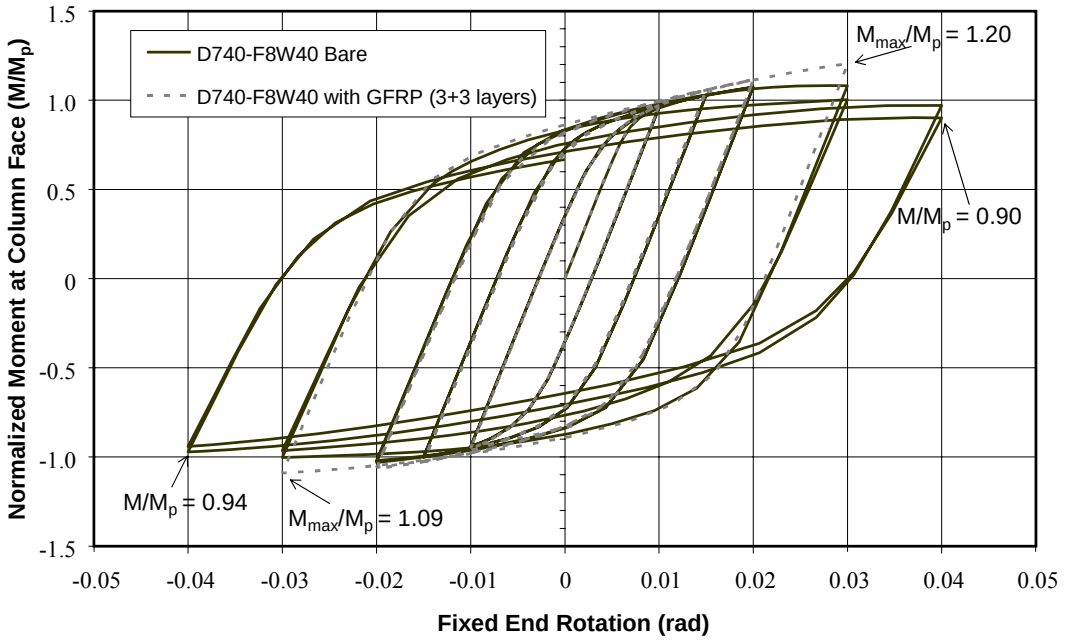

Figure 4.6 M/M_p-Θ relationships of D740-F8W40 section with and without GFRP

Table 4.3 FEA Results for Sections with Depth/Width Ratio of 2.79

	1	2	3	4	5	6	7	8	9	10	11	12	13
	Section Designation	# of Layers (Total thickness of GFRP)	t_{GFRP}	Last Rotation/Cycle Prior to Local Buckling				M_{max}/M_p for Sections with GFRP		M/M_p @ the end of 2nd Cycle of 0.04 rad of Rotation for Bare Sections		Max Shear Stresses @ Last Rotation/Cycle Prior to Local Buckling	
				Negative Bending		Positive Bending							
				Bare Section	Section w/ GFRP	Bare Section	Section w/ GFRP	Negative Bending	Positive Bending	Negative Bending	Positive Bending	Interfacial	Interlaminar
1	D740-F8W40	3+3 (5.4 mm)	$0.33t_f$	0.020/1st	0.020/2nd	0.020/2nd	0.025/1st	1.09	1.20	0.94	0.90	13.0	13.1
2	D740-F8W45	3+3 (5.4 mm)	$0.33t_f$	0.020/1st	0.020/2nd	0.020/2nd	0.025/1st	1.06	1.12	0.91	0.87	13.4	14.6
3	D740-F8W50	3+3 (5.4 mm)	$0.33t_f$	0.015/2nd	0.020/1st	0.020/1st	0.020/2nd	1.05	1.10	0.89	0.88	13.3	14.1
4	D740-F8W55	3+3 (5.4 mm)	$0.33t_f$	0.015/2nd	0.018/1st	0.020/1st	0.020/2nd	1.00	1.09	0.88	0.86	13.3	14.3
5	D740-F8W60	3+3 (5.4 mm)	$0.33t_f$	0.015/1st	0.015/2nd	0.015/2nd	0.020/1st	0.99	1.07	0.86	0.84	14.3	14.6
6	D740-F9W40	3+3 (5.4 mm)	$0.37t_f$	0.015/1st	0.015/2nd	0.020/2nd	0.023/1st	1.04	1.18	0.91	0.84	12.4	13.9
7	D740-F9W45	3+3 (5.4 mm)	$0.37t_f$	0.015/1st	0.015/2nd	0.020/2nd	0.023/1st	1.03	1.09	0.88	0.84	12.7	13.9
8	D740-F9W50	3+3 (5.4 mm)	$0.37t_f$	0.015/1st	0.015/2nd	0.020/1st	0.020/2nd	0.99	1.08	0.86	0.84	13.1	14.1
9	D740-F9W55	3+3 (5.4 mm)	$0.37t_f$	0.015/1st	0.015/2nd	0.017/1st	0.020/1st	0.99	1.08	0.85	0.82	13.4	15.0
10	D740-F9W60	3+3 (5.4 mm)	$0.37t_f$	0.015/1st	0.015/2nd	0.015/2nd	0.017/1st	0.99	1.05	0.84	0.79	13.3	13.6
11	D740-F10W40	3+3 (5.4 mm)	$0.41t_f$	0.015/2nd	0.015/2nd	0.020/1st	0.020/1st	1.01	1.09	0.87	0.83	11.9	13.9
12	D740-F10W45	3+3 (5.4 mm)	$0.41t_f$	0.015/2nd	0.015/2nd	0.020/1st	0.020/1st	0.99	1.08	0.85	0.78	12.3	13.8
13	D740-F10W50	3+3 (5.4 mm)	$0.41t_f$	0.015/1st	0.015/2nd	0.018/1st	0.020/1st	0.99	1.08	0.81	0.78	12.6	13.8
14	D740-F10W55	3+3 (5.4 mm)	$0.41t_f$	0.015/1st	0.015/2nd	0.015/2nd	0.020/1st	0.98	1.07	0.81	0.77	12.9	13.8
15	D740-F10W60	3+3 (5.4 mm)	$0.41t_f$	0.014/1st	0.015/2nd	0.015/2nd	0.016/1st	0.97	1.02	0.81	0.76	13.3	13.8

4.3.3.2 Sections with Depth/Width Ratio of 2.10

Table 4.4 presents results from the M/M_p-Θ behaviors of sections with depth/width ratio of 2.10. For bare sections the rotation capacities that were achieved without any local buckling or strength degradation were around 0.030 rad and 0.020 rad for positive and negative bendings, respectively. Observing the results presented in columns 10 and 11 revealed that the strength degradations at the end of 2nd cycle of 0.04 rad of rotation were more than 20% for almost all of the sections. Only section D556-F8W40 experienced degradations below 20%. All of the other sections suffered strength degradations in excess of 20% either only at negative bending or at both negative and positive bendings. Using 3+3 layers of GFRP strips for sections with FSR of 8 and 9 caused the interlaminar shear strength of GFRP strips to be exceeded. Therefore, 2+2 layers of GFRP strips were the thickest layer that could be used for these sections without the interlaminar shear strength being exceeded. For sections with an FSR of 10 3+3 layers of GFRP strips could be used.

Comparing the rotation values prior to local buckling of bare sections with sections with GFRP (columns 4, 5, 6, and 7) revealed that in negative bending the addition of GFRP strips did not increase the rotation capacity of the sections. Only sections D556-F10W40 and D-556-F10W45 showed a slight increase, which was not significant to consider. In positive bending four out of the six sections showed an increase in the rotation capacity. The rotation capacities in positive bending of sections D556-F8W45 / F8W50 / F9W50 / F10W40 increased to 2nd cycle of 0.03 rad, 2nd cycle of 0.03 rad, 1st cycle of 0.03 rad, and 1st cycle of 0.025 rad, respectively. The maximum normalized column face moment of sections with GFRP was 1.15, which was achieved by section D556-F8W40 in positive bending.

Table 4.4 FEA Results for Sections with Depth/Width Ratio of 2.10

	1	2	3	4	5	6	7	8	9	10	11	12	13
	Section Designation	# of Layers (Total thickness of GFRP)	t_{GFRP}	Last Rotation/Cycle Prior to Local Buckling				M_{max}/M_p for Sections with GFRP		M/M_p @ the end of 2nd Cycle of 0.04 rad of Rotation for Bare Sections		Max Shear Stresses @ Last Rotation/Cycle Prior to Local Buckling	
				Negative Bending		Positive Bending							
				Bare Section	Section w/ GFRP	Bare Section	Section w/ GFRP	Negative Bending	Positive Bending	Negative Bending	Positive Bending	Interfacial	Interlaminar
1	D556-F8W40	2+2 (3.6 mm)	$0.22t_f$	0.020/2nd	0.020/2nd	0.035/1st	0.035/1st	1.01	1.15	0.84	1.01	10.5	16.4
2	D556-F8W45	2+2 (3.6 mm)	$0.22t_f$	0.020/2nd	0.020/2nd	0.030/1st	0.030/2nd	0.97	1.06	0.79	0.86	10.9	16.3
3	D556-F8W50	2+2 (3.6 mm)	$0.22t_f$	0.020/2nd	0.020/2nd	0.030/1st	0.030/2nd	0.96	1.07	0.76	0.82	10.8	15.9
4	D556-F9W40	2+2 (3.6 mm)	$0.22t_f$	0.020/1st	0.020/1st	0.030/1st	0.030/1st	0.93	1.05	0.72	0.86	10.4	16.5
5	D556-F9W45	2+2 (3.6 mm)	$0.22t_f$	0.020/1st	0.020/1st	0.030/1st	0.030/1st	0.91	1.04	0.69	0.80	10.6	16.2
6	D556-F9W50	2+2 (3.6 mm)	$0.22t_f$	0.020/1st	0.020/1st	0.020/2nd	0.030/1st	0.9	1.03	0.66	0.77	10.7	15.8
7	D556-F10W40	3+3 (5.4 mm)	$0.41t_f$	0.015/2nd	0.018/1st	0.020/2nd	0.025/1st	0.91	1.04	0.67	0.80	10.1	13.5
8	D556-F10W45	3+3 (5.4 mm)	$0.41t_f$	0.015/2nd	0.018/1st	0.020/2nd	0.020/2nd	0.89	0.99	0.62	0.76	10.4	13.6
9	D556-F10W50	3+3 (5.4 mm)	$0.41t_f$	0.015/2nd	0.015/2nd	0.020/2nd	0.020/2nd	0.87	0.96	0.60	0.71	10.8	13.3

4.3.3.3 Sections with Depth/Width Ratio of 1.38

Table 4.5 presents results from the M/M_p-Θ behaviors of sections with depth/width ratio of 1.38. The results presented in column 4 and 6 reveal that the rotation capacities of the bare sections prior to local buckling were around 0.04 rad and 0.03 rad for positive and negative bending, respectively. In addition, the strength degradations of the bare sections at the end of 2nd cycle of 0.04 rad of rotation were below 20%. For sections D365-F8W30 / F8W35 / F8W40 / F9W35 / F9W40 the addition of even 1+1 layers of GFRP strips caused the interfacial shear strength of the bond surface between steel and GFRP to be exceeded prior to local buckling of the flanges. For sections D365-F9W35 / F10W30 / F10W35 / F10W40 interfacial shear stresses developed at the bond surface between steel and 1+1 layers of GFRP remained below the accepted interfacial shear strength. Although the interfacial shear strength was not exceeded for sections these sections with 1+1 layers of GFRP strips, the GFRP reinforcement still did not improve the rotation capacities of these three sections, as can be observed by comparing the rotation values presented in columns 4-5 and 6-7.

Table 4.5 FEA Results for Sections with Depth/Width Ratio of 1.38

	1	2	3	4	5	6	7	8	9	10	11	12	13
	Section Designation	# of Layers (Total thickness of GFRP)	t_{GFRP}	Last Rotation/Cycle Prior to Local Buckling				M_{max}/M_p for Sections with GFRP		M/M_p @ the end of 2nd Cycle of 0.04 rad of Rotation for Bare Sections		Max Shear Stresses @ Last Rotation/Cycle Prior to Local Buckling	
				Negative Bending		Positive Bending							
				Bare Section	Section w/ GFRP	Bare Section	Section w/ GFRP	Negative Bending	Positive Bending	Negative Bending	Positive Bending	Interfacial	Interlaminar
1	D365-F8W30	1+1 (1.8 mm)	$0.11t_f$	0.030/2nd	0.030/2nd	0.040/2nd	0.040/2nd	N/A	N/A	0.98	1.06	15.5	N/A
2	D365-F8W35	1+1 (1.8 mm)	$0.11t_f$	0.030/2nd	0.030/2nd	0.040/2nd	0.040/2nd	N/A	N/A	0.94	1.05	15.7	N/A
3	D365-F8W40	1+1 (1.8 mm)	$0.11t_f$	0.030/2nd	0.030/2nd	0.040/1st	0.040/1st	N/A	N/A	0.92	1.05	16.0	N/A
4	D365-F9W30	1+1 (1.8 mm)	$0.11t_f$	0.030/1st	0.030/1st	0.040/1st	0.040/1st	N/A	N/A	0.92	1.00	14.8	N/A
5	D365-F9W35	1+1 (1.8 mm)	$0.11t_f$	0.030/1st	0.030/1st	0.040/1st	0.040/1st	N/A	N/A	0.90	0.98	15.2	N/A
6	D365-F9W40	1+1 (1.8 mm)	$0.11t_f$	0.030/1st	0.030/1st	0.040/1st	0.040/1st	N/A	N/A	0.87	0.95	15.4	N/A
7	D365-F10W30	1+1 (1.8 mm)	$0.11t_f$	0.030/1st	0.030/1st	0.030/2nd	0.030/2nd	N/A	N/A	0.88	0.94	14.3	N/A
8	D365-F10W35	1+1 (1.8 mm)	$0.11t_f$	0.020/2nd	0.020/2nd	0.030/2nd	0.030/2nd	0.86	0.97	0.85	0.92	10.6	N/A
9	D365-F10W40	1+1 (1.8 mm)	$0.11t_f$	0.020/2nd	0.020/2nd	0.030/2nd	0.030/2nd	0.86	0.97	0.84	0.90	11.0	N/A

CHAPTER 5

CONCLUSIONS

An analytical study was conducted to improve the understanding of the cyclic behavior of steel I-beams modified by a welded haunch at the bottom flange and reinforced with GFRP strips at the plastic hinge region. Modified steel sections with flange slenderness ratios of 8, 9, and 10, which exceeded the slenderness limits set forth in current seismic design codes were investigated. Different web slenderness and depth/width ratios were considered. The elastic modulus of GFRP, interfacial shear strength of the bond surface between steel and GFRP, and interfacial shear strength of the GFRP strips were taken as 10000 MPa, 15.0 MPa, and 18.0 MPa, respectively. The design moment of the beam column connection at the column face was taken as $1.2M_p$. The optimum length, width, and location of GFRP strips were d_b, $0.45b_f$, and configuration 3 as shown in Figure 4.3. One layer of GFRP was 0.9 mm thick. The following conclusions can be made based on the results obtained from the study:

1- The contribution of GFRP strips to the plastic local buckling behavior of steel beams modified by a bottom flange welded haunch was limited by either the interfacial shear strength of steel/GFRP bonded surface or interlaminar shear strength of GFRP strips. In order to minimize the interfacial and interlaminar shear stresses, GFRP strips should be attached to both sides of the flanges. Although a GFRP width of $0.45b_f$ was recommended for both sides of the flanges as seen in Figure 4.3, GFRP material could be bonded to the full width of the top of the top flange and bottom of bottom flange to further increase the bond area and decrease shear stresses. Using higher stiffness FRP materials or adding GFRP strips to the webs were not effective in decreasing the interfacial or interlaminar shear stresses.
2- The rotation capacities prior to local flange buckling of modified bare steel sections increased as the depth/width ratio of the sections decreased. While modified bare

sections with depth/width ratio of 2.79 could reach rotations in the order of 0.02 radians prior to local buckling, the rotation capacities of modified bare sections with depth/width ratio of 1.38 were in the order of 0.04 radians.

3- The decrease in the depth/width ratio of modified steel sections also caused the interfacial shear stresses at the bond surface between steel and GFRP to increase. This in return forced the number of layers of GFRP strips to be decreased in order to keep the interfacial shear stresses below the shear strength prior to flange local buckling. However, as the number of layers of GFRP strips decreases, their ability to brace local buckling also decreases. Hence, as seen from the results GFRP reinforcement was ineffective for shallow modified beams. For modified deep beam sections with depth/width ratio of 2.79 3+3 layers of GFRP strips were the thickest that could be used without exceeding the interfacial and interlaminar shear strength values prior to local flange buckling. The number of layers that could be used without exceeding the interfacial and interlaminar shear strengths prior to local flange buckling dropped to 1+1 for shallow beams with a depth/width ratio of 1.38.

4- For deep modified beams (2 < depth/width < 3) the contribution of GFRP strips on mitigation of local flange buckling increases as the depth/width ratio increases and flange/web slenderness ratios decrease. 3+3 and 2+2 number of layers of GFRP should be used for deep modified beams with depth/width ratio closer to 3 and 2, respectively. The rotation values that can be maintained without experiencing local flange buckling by the appropriate GFRP reinforcement are summarized below:

   a) Modified beam sections with depth/width ratio close to 3, FSR of 8, WSR between 40-55: 0.02 radians for both positive and negative bending.

   b) Modified beam sections with depth/width ratio close to 3, FSR of 9 and 10, WSR between 40-55: 0.02 radians for positive bending, 0.015 radians for negative bending.

   c) Modified beam sections with depth/width ratio close to 3, FSR of 9 and 10, WSR of 60: 0.015 radians for both positive and negative bending.

   d) Modified beam sections with depth/width ratio close to 2, FSR of 8, WSR between 40-50: 0.03 radians for positive bending and 0.02 radians for negative bending.

e) Modified beam sections with depth/width ratio close to 2, FSR of 9 and 10: No considerable contribution.

5- It is not possible to rely on GFRP reinforcement to increase the flexural resistance of modified beam column connections at a rotation of 0.04 radians. The bond between steel and GFRP will fail in rotations much lower than 0.04 radians. However, if the bottom flange welded haunch modification is applied in an effort to moderately improve the seismic performance of the structure, then GFRP reinforcement can help the connections to maintain rotations in the order of 0.02 radians, which is required for intermediate moment frames, and may eliminate cumbersome repair works of buckled flanges and webs.

REFERENCES

Accord, N.B. and Earls, C.J. 2006. Use of fiber reinforced polymer composite elements to enhance structural steel member ductility. *Journal of Composites for Construction*, ASCE, 10(4):337-344.

Alkan, D. 2008. *Numerical Study of Enhancement of Plastic Rotation Capacity of Seismic Steel Moment Connections by Fiber Reinforced Polymer Materials*. Master of Science Thesis, Izmir Institute of Technology (IYTE), October.

ANSYS User Manual, *Swanson Analysis Systems, Inc*., 2007.

AISC. 2001. *Modification of Existing Weld Steel Moment Frame connections for Seismic Resistance. Steel Design Guide Series12.* American Institute of Steel Construction (AISC), Chicago, IL.

AISC. 2005. *Seismic provisions for structural steel buildings, American Institute of Steel Construction* (AISC), Chicago, IL.

Boone, M.J. 2002. Mechanical Testing of Epoxy Adhesives for Naval Applications, *Master of Science Thesis, The Graduate School of The University of Maine*, December.

Buyukozturk, O., Gunes, O., and Karaca, E. 2004. Progress on Understanding Deponding Problems in Reinforced Concrete and Steel Members Strengthened Using FRP Composites. *Construction and Building Materials* 18(1):9-19.

Cadei, J.M., Stanford, T.J., and Hollaway, T.C., eds. 2004. *Strengthening Metallic Structures Using Externally Bonded Fiber-Reinforced Polymers. Publication C595, Construction Industry Research and Information Association* (CIRIA), London, UK:233.

Chen, W.F. and Han, D.J. 1988. *Plasticity for Structural Engineers.* New York: Springer-Verlag.

Dawood, M. and Rizkalla, S. 2006. Bond and Splice Behavior of High Modulus CFRP Materials Bonded to Steel Structures. *Third International Conference on FRP Composites in Civil Engineering*, December, Miami, Florida.

Eğilmez, O.Ö. *2009. 4th Progress report, TUBITAK*, Project No: 106Y309.

Ekiz, E., El-Tawil, S., Parra-Montesinos, G., and Goel, S. 2004. Enhancing Plastic Hinge Behavior in Steel Flexural Members Using CFRP Wraps, *Proceedings of the 13rd World Conference on Earthquake Engineering*: 2496.

Eurocode-8. 2003. *Design of Structures for Earthquake Resistance – Part-1: General Rules, Seismic Actions, and Rules for Buildings*. Brussels, Belgium: *European Committee for Standardization* (CEN).

FEMA (Federal Emergency Management Agency) 2000a. *Recommended Seismic Design Criteria for New Steel Moment-Frame Buildings*. Washington, D.C: Federal Emergency Management Agency (FEMA) Publication No. - FEMA-350.

FEMA (Federal Emergency Management Agency) 2000b. *Recommended Seismic Evaluation and Upgrade Criteria for Existing Welded Steel Moment-Frame Buildings.* Washington, D.C: Federal Emergency Management Agency (FEMA) Publication No. FEMA-351.

Gibson, R.F. 1994. *Principles of Composite Material Mechanics*. New York: McGrawHill.

Güven, C. A. 2009. *Experimental Study on Improving Local Buckling Behavior of Steel Plates Strengthened with Glass Fiber Reinforced Polymers*. Master of Science Thesis, Izmir Institute of Technology (IYTE), April.

Hull, D. and Clyne, T.W. 2000. *An Introduction to Composite Materials*. Cambridge: Cambridge University Press, 2nd Editon.

Jones, R.M. 1998. *Mechanics of Composite Materials*. Philadelphia, PA: Taylor & Francis, 2nd Edition.

Lenwari, A., Thepchatri, T., and Albrecht, P. 2005. Flextural Response of Steel Beams Strengthened with Partial-Length CFRP Plates. *Journal of Composites for Construction* 9(4):296-303

Lili, S., Yan, Z., Yuexin, D. Ve Zuoguang Z. 2008. Interlaminar Shear Property of Modified Glass Fiber Reinforced Polymer with Different MWCNTs. *Chinese Journal of Aeronautics,* ELSEVIER, 21(2008):361-369.

Nakashima, M., Suita, K., Morisako, K. 1998. Tests of Welded Beam-Column Subassemblies I: Global Behavior. *Journal of Structural Engineering*, ASCE 124(11):1236-1244.

Nakashima, M., Kanao, I., Liu, D. 2002. Lateral Instability and Lateral Bracing of Steel Beams Subjected to Cyclic Loading. *Journal of Structural Engineering*, ASCE 128(10):1308-1316.

Nakashima, M., Liu, D., Kanao, I. 2003. Lateral-Torsional and Local Instability of Steel Beams Subjected to Large Cyclic Loading. *Journal of Steel Structures, Korean Society of Steel Construction* 3(3):179-189.

Okazaki, T., Liu, D., Nakashima, M., and Engelhardt, M.D. 2006. Stability Requirements for Beams in Seismic Steel Moment Frames. *Journal of Structural Engineering*, ASCE 132(9):1331-1342.

Photiou, N.K., Hollaway, L.C., and Chryssanthopoulos, M.K. 2006. Strengthening of an Artificial Degraded Steel Beam Utilizing a Carbon/Glass Composite System. *Construction and Building Materials* 20:11-21.

Richard, D.H. 2004. *Mchanical Properties of Matarials Data* MK-HDBK-5E:9-23. http://www.engr.ku.edu/~rhale/ae510/elasticity/sld009.htm (accessed May 15, 2008).

SAC. (1996). *Experimental investigation of beam-column subassemblages. Technical Report* SAC-96-01, Parts 1 and 2, Sacramento, CA:SAC Joint Venture.

Sayed-Ahmet, E.Y. 2004. Strengthening of Thin-Walled Steel I-Section Beams Using CFRP Strips. *Proceedings of the 4th Advanced Composites for Bridges and Structures Conference*, Calgary, Canada.

Schwartz, M.M. 2002. *Composite Materials*. New Jersey: Prentice Hall PTR.

Schnerch, D., Dawood, M., Rizkalla, S., and Sumner, E. 2007. Proposed Design Guidelines for Strengthening of Steel Bridges with FRP Materials. *Construction and Building Materials* 21:1001-1010.

Setunge, S., Kumar, A., and Nezamian, A., eds. 2002. *Review of Strengthening Techniques Using Externallay Bonded Fiber Reinforced Polymer Composites*. Report 2002-005-C-01. Australia: CRC for Construction Innovation.

Tavakkolizadeh, M. and Saadatmanesh, H.2003. Strengthening of Steel-Concrete Composite Girders Using Corbon Fiber Reinforced Polymers Sheets. *Journal of Structural Engineering* (ASCE) 126(1):30-40.

TCBİB. 2006. *Specification for Structures to be Built in Disaster Areas*. Ankara, Turkey.

Uang, C.M. and Fan, C.C. 2002. Stability Criteria for Steel Moment Connections with Reduced Beam Section. *Journal of Structural Engineering* 127(9):1021-1027.

Yu, Q.S., Uang, C.M., and Gross, I.L. 2000. SeismicRehabilitation Design of Steel Moment Connection with Welded Haunch. *Journal of Structural Engineering* (ASCE) 126(1):57-68.